Taylor & Francis
Taylor & Francis Group

Journal of Vertebrate Paleontology

ISSN: 0272-4634 (Print) 1937-2809 (Online) Journal homepage: https://www.tandfonline.com/loi/ujvp20

Yaquinacetus meadi, a new latest Oligocene–early Miocene dolphin (Cetacea, Odontoceti, Squaloziphiidae, fam. nov.) from the Nye Mudstone (Oregon, U.S.A.)

Olivier Lambert, Stephen J. Godfrey & Erich M. G. Fitzgerald

To cite this article: Olivier Lambert, Stephen J. Godfrey & Erich M. G. Fitzgerald (2019): *Yaquinacetus meadi*, a new latest Oligocene–early Miocene dolphin (Cetacea, Odontoceti, Squaloziphiidae, fam. nov.) from the Nye Mudstone (Oregon, U.S.A.), Journal of Vertebrate Paleontology

To link to this article: https://doi.org/10.1080/02724634.2018.1559174

Journal of Vertebrate Paleontology e1559174 (19 pages)

DOI: 10.1080/02724634.2018.1559174

ARTICLE

YAQUINACETUS MEADI, A NEW LATEST OLIGOCENE–EARLY MIOCENE DOLPHIN (CETACEA, ODONTOCETI, SQUALOZIPHIIDAE, FAM. NOV.) FROM THE NYE MUDSTONE (OREGON, U.S.A.)

OLIVIER LAMBERT, *[,1] STEPHEN J. GODFREY,[2,3] and ERICH M. G. FITZGERALD[4,5]
[1]Direction Opérationnelle Terre et Histoire de la Vie, Institut royal des Sciences naturelles de Belgique, Rue Vautier, 29, 1000 Brussels, Belgium, olivier.lambert@naturalsciences.be;
[2]Department of Paleontology, Calvert Marine Museum, P.O. Box 97, Solomons, Maryland 20688, U.S.A., stephen.godfrey@calvertcountymd.gov;
[3]Department of Paleobiology, National Museum of Natural History, Smithsonian Institution, Washington DC 20560, U.S.A.;
[4]Museums Victoria, G.P.O. Box 666, Melbourne, Victoria 3001, Australia, efitzgerald@museum.vic.gov.au;
[5]Department of Vertebrate Zoology, National Museum of Natural History, Smithsonian Institution, Washington, D.C. 20560, U.S.A.

ABSTRACT—Represented by a nearly complete cranium with associated mandible, teeth, and vertebrae, *Yaquinacetus meadi* is a new genus and species of archaic homodont odontocete from the latest Oligocene–early Miocene (24–19.2 Ma) of Oregon, U.S.A. The new species is characterized by a moderately elongated rostrum bearing approximately 51 alveoli per tooth row and a knob-like, rectangular vertex. Together with *Squaloziphius emlongi* from the early Miocene of Washington State, *Y. meadi* constitutes a new odontocete family, Squaloziphiidae, fam. nov., diagnosed by a unique combination of characters, including transversely wide dorsal opening of the mesorostral groove at base of rostrum, followed posteriorly by an abrupt narrowing; thickened lateral margin of the maxilla in the antorbital region making a long and laterally concave crest; and massive, anteroposteriorly and ventrally long postglenoid process of the squamosal. Although sharing with Ziphiidae the presence of transverse premaxillary crests on the vertex, Squaloziphiidae differs in the pterygoid sinus fossa being shorter anteriorly and ventrally; the tubercle of the malleus being less reduced; and lacking a pair of enlarged alveoli for mandibular tusks. Our phylogenetic analysis confirms the sister-group relationship between *S. emlongi* and *Y. meadi*, either as late diverging stem odontocetes or as early crown odontocetes, but distant from Ziphiidae. These results confirm the northeastern Pacific as a center of diversification for several groups of archaic homodont odontocetes during the late Oligocene–early Miocene.

http://zoobank.org/urn:lsid:zoobank.org:pub:9D12D4D3-EB46-4E6B-8AB4-1987B97EBC0F

SUPPLEMENTAL DATA—Supplemental materials are available for this article for free at www.tandfonline.com/UJVP

Citation for this article: Lambert, O., S. J. Godfrey, and E. M. G. Fitzgerald. 2019. *Yaquinacetus meadi*, a new latest Oligocene–early Miocene dolphin (Cetacea, Odontoceti, Squaloziphiidae, fam. nov.) from the Nye Mudstone (Oregon, U.S.A.). Journal of Vertebrate Paleontology. DOI: 10.1080/02724634.2018.1559174.

INTRODUCTION

When first described by Muizon (1991), the archaic odontocete (toothed whale) *Squaloziphius emlongi*, from the early Miocene of the Clallam Formation of Washington State, U.S.A., was proposed as the oldest known member of the modern family Ziphiidae (beaked whales), based on two cranial features: an elevated vertex with transverse premaxillary crests and the enlarged hamular process of the pterygoid; nevertheless, due to marked differences from other ziphiids, it was placed in its own subfamily Squaloziphiinae. Since then, several studies have questioned this taxonomic assignment (e.g., Fordyce and Barnes, 1994; Fordyce, 2002; Lambert and Louwye, 2006; Lambert et al., 2013; the former two suggesting affinities with the extinct Eurhinodelphinidae). Recent phylogenetic analyses offer differing results, with *Squaloziphius* appearing as one of the last stem odontocetes to branch off (Geisler and Sanders, 2003; Geisler et al., 2011, 2012, 2014; Gatesy et al., 2013; Godfrey et al., 2016; Vélez-Juarbe, 2017), as a separate lineage among crown odontocetes (Murakami et al., 2012; Aguirre-Fernández and Fordyce, 2014:fig. 8; Boersma and Pyenson, 2016; Tanaka and Fordyce, 2016, 2017; Lambert et al., 2018), or as sister group to Ziphiidae (e.g., Aguirre-Fernández and Fordyce, 2014:fig. 9; Lambert et al., 2015, 2017). The holotype of *S. emlongi* is an isolated partial skull, lacking most of the rostrum, the ear bones, and the mandible; new material, either from the same species or from a closely related taxon, thus has been long awaited in order to reassess the affinities of this enigmatic archaic odontocete.

A resolution may now be at hand in the form of another skull (USNM 214705, here designated as the type of a new genus and species) that, along with the holotype of *S. emlongi*, came to the National Museum of Natural History (Smithsonian Institution, Washington, D.C.) as part of the Emlong Collection. Originating in latest Oligocene–early Miocene deposits of the Nye Mudstone in Lincoln County, coastal Oregon, U.S.A., the holotype of the new taxon shares several characters with *S. emlongi* and fortunately is a much more complete specimen, preserving the full length of its rostrum, the ear bones, one mandible, and teeth. Its description and comparison call for placement of *S. emlongi* and the new taxon in a new family of extinct odontocetes, the Squaloziphiidae.

*Corresponding author.
Color versions of one or more of the figures in the article can be found online at www.tandfonline.com/ujvp.

Published online 22 Mar 2019

MATERIALS AND METHODS

Institutional Abbreviations—**ChM**, Charleston Museum, Charleston, South Carolina, U.S.A.; **CMM-V-**, Calvert Marine Museum vertebrate paleontology collection, Calvert County, Maryland, U.S.A.; **IRSNB**, Institut royal des Sciences naturelles de Belgique, Brussels, Belgium; **USNM**, United States National Museum of Natural History, Smithsonian Institution, Washington, D.C., U.S.A.

Anatomical Terminology—For the anatomy of the skull, we follow the terminology proposed by Mead and Fordyce (2009) for the extant delphinid *Tursiops*. For elements not recorded in *Tursiops* or not discussed in that publication, we try as much as possible to provide the source.

GEOLOGICAL SETTING

The specimen USNM 214705 was discovered in the Nye Mudstone, an approximately 1500-m-thick unit consisting of massive, organic-rich mudstone and siltstone deposited along coastal Oregon, U.S.A. (Prothero et al., 2001a). Based on magnetostratigraphy, the lower part of the Nye Mudstone is dated to the late Oligocene (28.0–26.0 Ma); planktonic microfossils (Zone M1a) and molluscs (Pillarian Molluscan Stage) suggest that the upper part of the unit dates from the early Miocene (Addicott, 1976; Prothero et al., 2001a; Nesbitt, 2018). The Nye Mudstone overlies the late Oligocene Yaquina Sandstone, whose top is dated to 28.0 Ma, and it is overlain by the late early to early middle Miocene Astoria Formation, whose base is dated to 19.2–20.7 Ma (Prothero et al., 2001a, 2001b). The geological age of the specimen USNM 214705 studied here is therefore broadly between 28 and 19.2 Ma (Chattian to earliest Burdigalian).

Based on the field notes of D. R. Emlong and the geological map of the area (Snavely et al., 1975:fig. 1; Fig. 1), the locality of USNM 214705 is closer to the contact of the Nye Mudstone with the overlying Astoria Formation than to the contact with the underlying Yaquina Sandstone; taking into account the magnetostratigraphic sample points of Prothero et al. (2001a, 2001b), the horizon of USNM 214705 can be further restricted to the upper part of the Nye Mudstone, in an estimated interval of 24–19.2 Ma (latest Chattian to earliest Burdigalian).

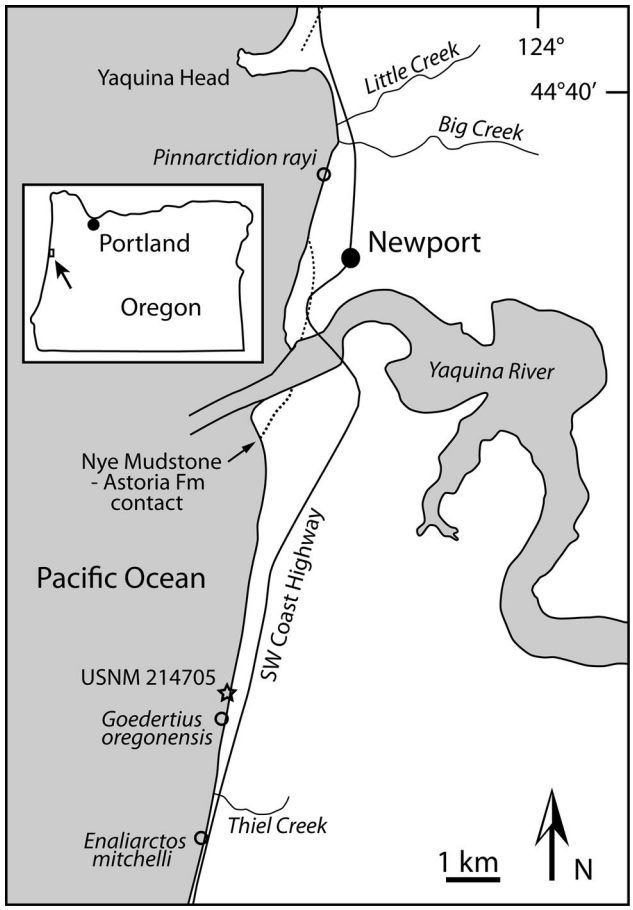

FIGURE 1. Schematic map of the coastal area around Newport, Lincoln County, Oregon, U.S.A., indicating the locality of the holotype of *Yaquinacetus meadi*, gen. et sp. nov., USNM 214705 (star), as well as the localities of the allodelphinid *Goedertius oregonensis* and the pinnipeds *Enaliarctos mitchelli* and *Pinnarctidion rayi*, all found in deposits of the Nye Mudstone, and the contact between Nye Mudstone and Astoria Formation at the mouth of the Yaquina River (following Snavely et al., 1975). Inset: position of the Newport area (arrow) in Oregon.

SYSTEMATIC PALEONTOLOGY

CETACEA Brisson, 1762
PELAGICETI Uhen, 2008
NEOCETI Fordyce and Muizon, 2001
ODONTOCETI Flower, 1867
SQUALOZIPHIIDAE (Muizon, 1991), fam. nov.

Type Genus—*Squaloziphius* Muizon, 1991.

Other Referred Genus—*Yaquinacetus*, gen. nov.

Diagnosis—Members of family Squaloziphiidae differ from other odontocetes, including archaic homodont species (e.g., '*Argyrocetus*' *bakersfieldensis*, '*Argyrocetus*' *joaquinensis*, *Chilcacetus cavirhinus*, *Macrodelphinus kelloggi*, and *Papahu taitapu*) in sharing the following unique combination of characters: transversely wide dorsal opening of mesorostral groove at base of rostrum, followed posteriorly by abrupt narrowing toward anterior margin of bony nares (synapomorphy); premaxillary foramen posterior to level of antorbital notch; lateral margin of premaxilla making a straight line from base of rostrum to posterior end of premaxillary sac fossa; thickened lateral margin of maxilla in antorbital region making a long and laterally concave crest; massive postglenoid process of squamosal, being longer ventrally than posttympanic process and exoccipital; apex of postglenoid process anteroposteriorly longer than transversely thick (synapomorphy); and prominent anterodorsal angle of periotic laterally shifted compared with anterior tip of anterior process (unknown in *Squaloziphius emlongi*). Although Squaloziphiidae share several derived characters with Ziphiidae (presence of transverse premaxillary crests on vertex, also present in several eurhinodelphinids and delphinidans, and transversely wide pterygoid sinus fossa), they further differ from the latter in pterygoid sinus fossa anteriorly not reaching the level of antorbital notch and ventrally distant from ventral-most level of basicranium; aperture for endolymphatic duct being dorsolateral to dorsal margin of spiral cribriform tract (unknown in *S. emlongi*); tubercule of malleus being less reduced (unknown in *S. emlongi*); and lacking a pair of enlarged alveoli for mandibular tusks (unknown in *S. emlongi*).

YAQUINACETUS, gen. nov.

Type and Only Included Species—*Yaquinacetus meadi*, gen. et sp. nov.

Diagnosis—As for type and only species.

Etymology—*Yaquinacetus*, a combination of 'Yaquina,' for the Yaquina River (and the Native American Yaquina tribe/people

formerly living along the river), reaching the Pacific Ocean a few kilometers north of the locality where USNM 214705 was discovered, and 'cetus,' whale in Latin. Gender masculine.

YAQUINACETUS MEADI, sp. nov.
(Figs. 2–9)

Holotype—USNM 214705, a nearly complete cranium (lacking only the left supraorbital), with associated ear bones (periotic, tympanic, malleus, incus, and stapes), right hemimandible, teeth, and lumbar and caudal vertebrae. Collected by Douglas R. Emlong in March 1969.

Type Locality—Following D. R. Emlong's field notes, the holotype was discovered in a bedrock covered by beach sand, about 150 feet (45.72 m) from the bank, approximately 3 miles (4.82 km) south of Newport and 3/4 mile (1.20 km) north of the mouth of Thiel Creek, Lincoln County, coastal Oregon, U.S.A. (Fig. 1). Approximate geographic coordinates: 44°34′30″N, 124°04′12″W. This locality is only a few hundred meters north of the mouth of Moore Creek, where the holotype of the allodelphinid odontocete *Goedertius oregonensis* and a partial skeleton of the bony-toothed bird *Pelagornis* sp. were found (Mayr et al., 2013; Kimura and Barnes, 2016), and about 1750 m north of the locality of the referred specimen USNM 175637 of the archaic pinniped *Enaliarctos mitchelli* (Berta, 1991). Additional marine tetrapods from the Nye Mudstone found in the Yaquina Bay area include a halitheriine dugongid (Domning and Ray, 1986), the littoral ursoid *Kolponomos newportensis* (Tedford et al., 1994), the phocoid pinniped *Pinnarctidion rayi* (Berta, 1994), a possible platanistine odontocete (Barnes, 2006), and a sea turtle (Brinkman, 2009).

Formation and Age—Nye Mudstone, upper part of the formation, latest Chattian to earliest Burdigalian (24–19.2 Ma; see discussion above).

Diagnosis—*Yaquinacetus meadi* is a medium-sized homodont odontocete characterized by a moderately elongated rostrum making up 60% of the condylobasal length and bearing approximately 51 alveoli in each upper tooth row; a knob-like, rectangular vertex; and an anteroposteriorly elongated temporal fossa. It differs from *Squaloziphius emlongi* in its smaller size (bizygomatic width of holotype = 241 mm); the premaxillary foramen being located more posteriorly, at the level of the anteromedial limit of bony nares; the presence of a single, large dorsal infraorbital foramen posterolateral to the antorbital notch; the proportionally wider vertex of the skull (ratio between minimum width of vertex and bizygomatic width = 0.16, as compared with 0.11 in *S. emlongi*); the more abruptly elevated vertex of the skull, with the ascending process of the premaxilla drawing an angle of about 45° with the dorsal surface of the rostrum at its base; the basioccipital crests being less posteriorly diverging (angle of 55–60°); and the less massive zygomatic and postglenoid processes of the squamosal.

Etymology—*meadi*, honoring James G. Mead (Curator Emeritus of Marine Mammals at USNM) for his multiple contributions to knowledge of the anatomy and ecology of cetaceans, especially beaked whales.

TABLE 1. Measurements (in mm) of the skull of the holotype of *Yaquinacetus meadi*, gen. et sp. nov., USNM 214705, including the cranium, left periotic, left and right tympanic bullae, left malleus, and mandible.

Dimension	Measurement
Cranium	
Condylobasal length	612
Rostrum length	365
Width of rostrum at mid-length	51
Width of premaxillae at rostrum mid-length	33
Width of rostrum at base	e114
Width of premaxillae at rostrum base	50
Maximum width of premaxillae in neurocranium region	65
Maximum width of right premaxilla at level of premaxillary sac fossa	29.5
Maximum width of left premaxilla at level of premaxillary sac fossa	30.5
Preorbital width	e190
Postorbital width	e236
Bizygomatic width	241
Maximum opening of mesorostral groove	25
Minimum distance between premaxillae anterior to bony nares	7
Width of bony nares	36.5
Maximum width of nasals	35
Maximum width of vertex across transverse premaxillary crests	65+
Minimum distance between maxillae across vertex	38
Orbit length	72
Length of temporal fossa	114
Height of temporal fossa	63+
Distance from anterior tip of zygomatic process to posteroventral margin of postglenoid process	109
Minimum distance between temporal crests across supraoccipital shield	e130
Width of occipital condyles	80
Width of foramen magnum	35
Distance between posterolateral margins of basioccipital crests	124
Left periotic	
Maximum length	e33.0
Maximum mediolateral width	19.6
Length of anterior process	7.8
Length of pars cochlearis (until anteromedial margin of fenestra rotunda)	12.7
Length of pars cochlearis (until posterodorsal margin of stapedial muscle fossa	17.0
Length of posterior process	e13.0
Tympanic bulla (left/right)	
Total length (without posterior process)	35.0/35.0
Maximum width	21.0/22.0
Maximum height of involucrum	14.0/—
Left malleus	
Maximum height	5.4
Maximum width perpendicular to maximum height	3.5
Mandible	
Total length	518+
Length of symphyseal portion	155+
Height at posterior end of symphyseal portion	28
Maximum length of tooth row	e290
Length of coronoid crest	e190
Maximum height of ramus	119
Distance from ventral margin of angular process to mandibular condyle	32
Height of mandibular condyle	e43

e, estimate; +, not complete; —, no data.

DESCRIPTION

Cranium, Overview—The cranium of USNM 214705 has smaller dimensions than the holotype of *Squaloziphius emlongi*; for example, the bizygomatic width is 241 mm, versus 296 mm in the latter (Table 1; Muizon, 1991). The cranium presents a gracile and moderately elongated rostrum (60% of condylobasal length) displaying homodont dentition (Figs. 2 and 4). The whole rostrum is wider than high in transverse section, with a wide dorsal exposure of the maxilla; the anterior part of the rostrum is markedly dorsoventrally flattened, a feature only partly explainable by burial/fossilization processes. The mesorostral groove is widely open dorsally for the whole length of the rostrum, differing in that morphology from the more restricted mesorostral groove in *Chilcacetus* and *Macrodelphinus* (Wilson, 1935; Lambert et al., 2015). The premaxillary sac fossae are essentially symmetrical. The vertex of the cranium is elevated, knob-like, and slightly shifted to the left as compared with the sagittal plane of the cranium. Some of this left-shift may be due to slight dorsoventral deformation of the

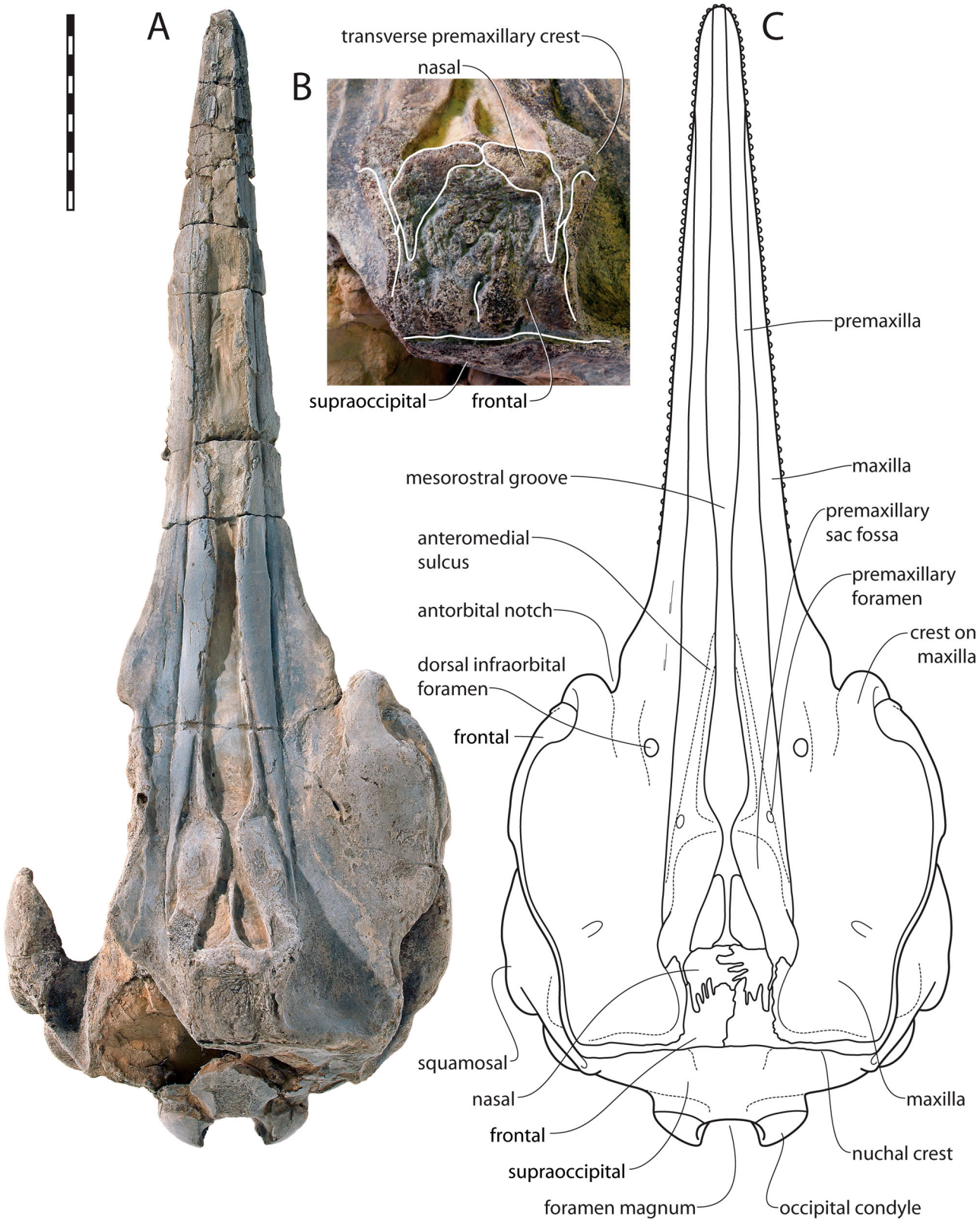

FIGURE 2. Cranium of the holotype of *Yaquinacetus meadi*, gen. et sp. nov., USNM 214705. **A**, dorsal view; **B**, vertex in dorsal view, with an alternative interpretation of the sutures (see text for details); **C**, reconstruction of the cranium in dorsal view. The fossil was lightly coated with sublimed ammonium chloride. Scale bar equals 100 mm.

neurocranium, as evidenced by the presence of breaks along the supraoccipital shield and on the medial wall of the temporal fossa. The temporal fossa is anteroposteriorly long; it is only moderately elevated, distinctly lower than the vertex.

Premaxilla—The premaxilla-maxilla suture is visible anteriorly until 40 mm from the rostral apex. Therefore, the anterior premaxillary portion of the rostrum was short (much shorter than in eurhinodelphinids and *Chilcacetus*). The alveolar groove extends to the rostral apex, with shallow, poorly preserved alveoli (Fig. 3). Along the rostrum, the premaxilla-maxilla suture is not in a lateral groove, unlike the distinct groove present in allodelphinids, eoplatanistids, eurhinodelphinids, and platanistids. The premaxilla partly dorsally overhangs the broad mesorostral groove on the posterior third of the rostrum, with a minimum distance between the premaxillae of 70 mm anterior to the level of the antorbital notch (Figs. 2, 5A). Behind this point, the medial margins of the premaxillae diverge until a maximum separation is reached slightly beyond the level of the antorbital notch. In this region, the dorsal surface of the premaxilla is smooth and made of compact bone (porcelanous part sensu Mead and Fordyce, 2009). From that level, the medial margin of the premaxilla curves abruptly posteromedially toward the anteromedial corner of the premaxillary sac fossa. A similar abrupt narrowing of the dorsal opening of the mesorostral groove is present in *Squaloziphius*, whereas it is either more gradual or absent in the eurhinodelphinids, '*Argyrocetus*' *bakersfieldensis*, '*A.*' *joaquinensis*, *Chilcacetus*, *Macrodelphinus*, and *Papahu*. Closer to the lateral margin of the premaxilla than to the medial margin, the premaxillary foramen is far posterior (about 40 mm) to the level of the antorbital notch (Fig. 2C). Emerging anteriorly from the aforementioned foramen is the anteromedial sulcus, which is much longer than in *Squaloziphius* (possibly related to the relatively more posterior position of the premaxillary foramen in *Yaquinacetus*). The slightly transversely convex dorsal surface of the prenarial triangle rises steeply dorsomedially. Laterally bordered by a distinct posterolateral sulcus until a level behind the mid-length of the bony nares, the premaxillary sac fossa is longitudinally short (somewhat shorter than in *Squaloziphius*); as in *Squaloziphius*, it forms a thick pedestal, even thicker in the area medial to the premaxillary foramen. The medial part being more elevated, the fossa is transversely concave, differing from the planar to convex dorsal surface of the same in *Squaloziphius*. As in *Squaloziphius*, from the rostrum to the level of the posterior margin of the bony nares, the premaxilla-maxilla suture is rectilinear (Fig. 2), contrasting with the laterally bowed suture in the premaxillary sac fossa region of many other odontocetes. The narrow bony nares are anteriorly pointed.

In lateral view, the elevation of the premaxilla toward the vertex is pronounced (Fig. 4); the dorsal surface of the ascending process draws an angle of about 45° with the dorsal surface of the base of the rostrum. This angle is greater than in *Squaloziphius*. Lateral and medial margins of the ascending process of the premaxilla are parallel in anterodorsal view (Fig. 5A, B), lacking the constriction seen in most ziphiids (with the exception of berardiines). The ascending process retains its transverse width until the vertex, with the dorsolateral margin overhanging the maxilla (a feature best seen in posterodorsal view; Fig. 5D). The dorsal surface of the resulting narrow transverse premaxillary crest is abraded, revealing spongy bone; it was originally somewhat dorsoventrally thicker. Also present in *Squaloziphius* (Muizon, 1991), this transverse premaxillary crest is similar to the crest observed in berardiine ziphiids (e.g., *Archaeoziphius* and *Berardius*). A less developed crest is seen in a few eurhinodelphinids and in some delphinidans (e.g., *Australodelphis* and *Macrokentriodon*) (Dawson, 1996; Fordyce et al., 2002; Lambert, 2005). On the vertex, the premaxilla may have had a narrow and long projection between the nasal and the maxilla, contacting the frontal (Fig. 2B, C). In an alternative interpretation, the premaxilla is shorter lateral to the nasal and does not contact the frontal. The posterolateral plate of the premaxilla (sensu Fordyce, 1994) is well defined.

Maxilla—At the base of the rostrum, the maxilla flares posterolaterally, reaching the transverse level of the antorbital notch 27 mm anterior to the notch on the right side. This laterally convex and somewhat dorsally elevated lateral margin of the rostrum at its base differs from the seemingly more rectilinear and dorsoventrally thinner margin in *Squaloziphius*. Limited information is available about the rostrum of *Squaloziphius*; considering the differences from *Yaquinacetus* at the base of rostrum, the latter may not be the most relevant model for a reconstruction of the snout of *Squaloziphius*. The antobital notch is narrow and 'V'-shaped. A single, moderately large dorsal infraorbital foramen lies posteromedial to the antorbital notch; it contrasts with the smaller and more numerous foramina observed in that area for *Squaloziphius*. Anterior to the antorbital notch, two tiny foramina are present on the left maxilla, each anteriorly extended by a fine sulcus. A posterior dorsal infraorbital foramen pierces the maxilla at the longitudinal level of the bony nares, closer to the lateral margin of the maxilla than to the premaxilla. In the antorbital region, the right maxilla anteriorly is 17 mm longer than the frontal; there, the lateral margin of the maxilla is distinctly thickened, making a crest that curves anterolaterally, in a way similar to the condition in *Macrodelphinus* and *Squaloziphius*. Being located posterolateral to the antorbital notch, this maxillary crest is not homologous to the more medial rostral maxillary crest observed in many ziphiids; it occupies roughly the same position as the maxillary crest of *Kogia* (Mead and Fordyce, 2009:diagram 2) but is not associated with a supracranial basin. In the supraorbital region, most of the frontal is covered by the maxilla. The latter reaches the nuchal crest, where its posterior margin makes a straight line. In lateral view (Fig. 4), the posterolateral corner of the maxilla is slightly posterior to and much lower than the posteromedial corner, different from the condition in *Chilcacetus* and *Macrodelphinus* (the two corners at about the same vertical level in these taxa). The maxilla and frontal do not completely hide the squamosal from dorsal view. The lateral wall of the vertex is vertical and high.

Polydonty is well developed in *Yaquinacetus*; taking into account the few anterior alveoli that may belong to the premaxilla, each upper alveolar groove has an estimated count of 51 alveoli for single-rooted teeth (Fig. 3). Circular anterior alveoli have a diameter ranging from 3.5 to 4 mm, with interalveolar septa 1–2 mm thick. The size of alveoli increases to 4–5 mm at mid-length of the rostrum and 4–4.5 mm posteriorly. The alveolar groove seemingly ends about 60 mm anterior to the antorbital notch.

Possibly increased due to postburial deformation, a broad medial depression separates left and right alveolar grooves in the anterior half of the ventral surface of the rostrum. The ventromedial surface of the palate is flat to slightly convex, lacking any keel. Starting from the anterior apex of the pterygoid, a low palatal ridge extends anteriorly and then turns anterolaterally before vanishing.

Several small foramina and short sulci are observed in the ventromedial region of the rostrum, between 105 and 180 mm from the anterior margin of the pterygoid sinus fossa. No major palatine foramen could be detected.

Nasal—Comprising the conjoined nasals, the posterior margin of the bony nares is posterior to the tip of the zygomatic process of the squamosal. With a convex dorsal surface, the nasals include the highest point of the cranium (Figs. 2 and 4). As preserved, the surface rises anterodorsally before lowering slightly toward the bony nares. However, the nasals are slightly abraded and may have originally projected anterodorsally to some extent, as in '*Argyrocetus*' *bakersfieldensis*, *Chilcacetus*,

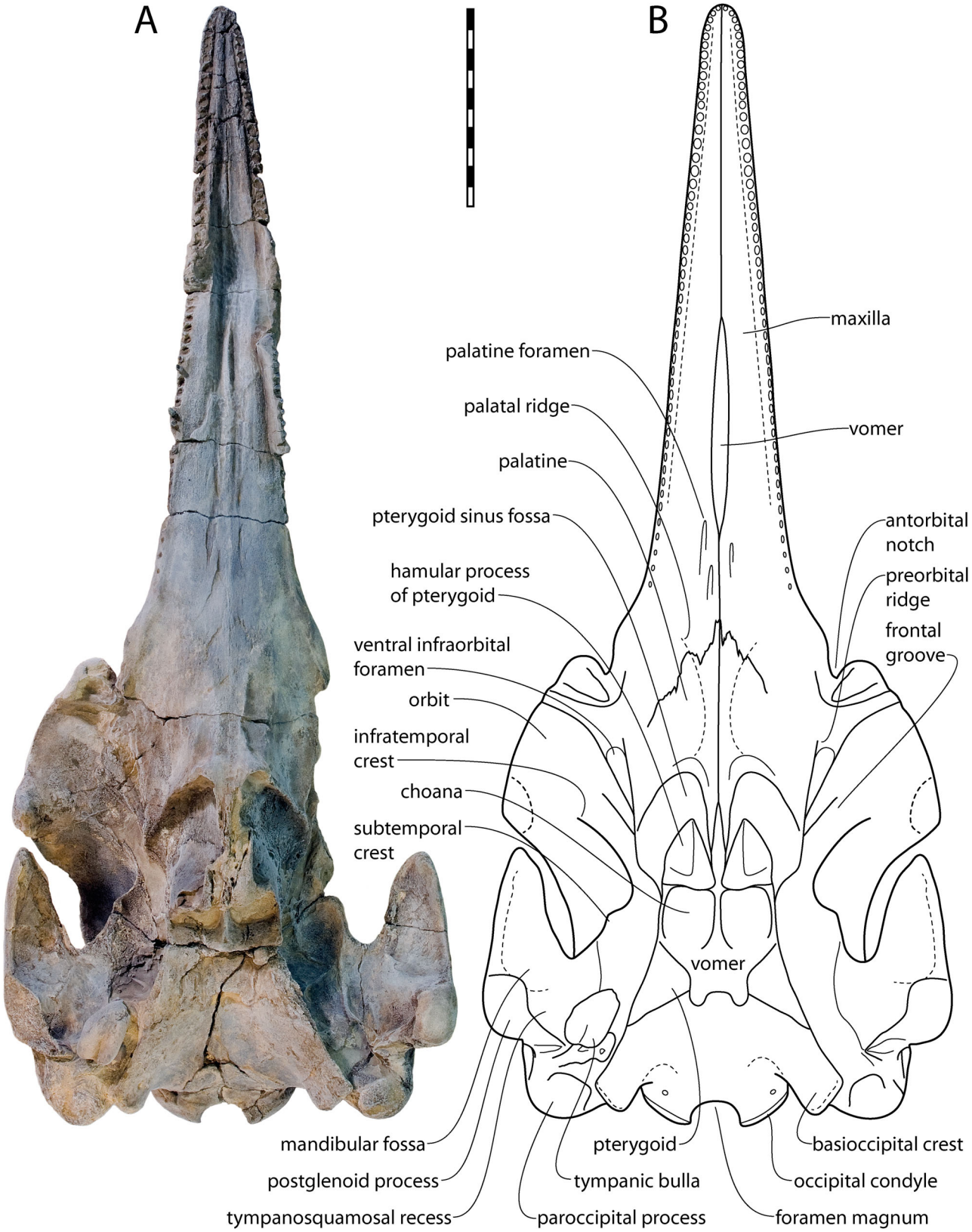

FIGURE 3. Cranium of the holotype of *Yaquinacetus meadi*, gen. et sp. nov., USNM 214705. **A**, ventral view; **B**, reconstruction of same. The fossil was lightly coated with sublimed ammonium chloride. Scale bar equals 100 mm.

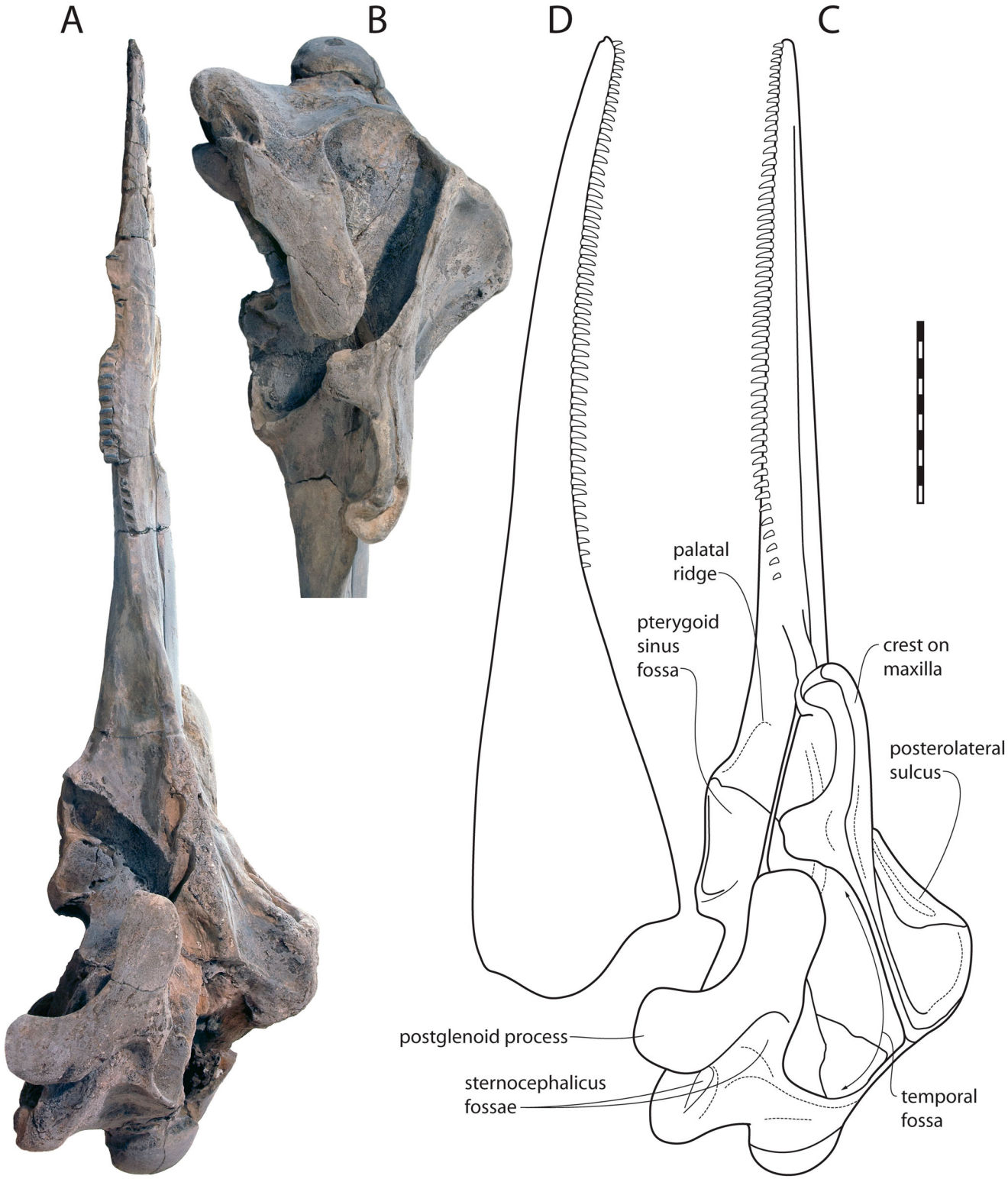

FIGURE 4. Skull of the holotype of *Yaquinacetus meadi*, gen. et sp. nov., USNM 214705. **A**, left lateral view of the cranium, with the left supraorbital region lacking; **B**, right lateral view of the neurocranium, with the right postglenoid process being incomplete; **C**, reconstruction of the cranium in left lateral view; **D**, reconstruction of the left hemimandible. The fossil was lightly coated with sublimed ammonium chloride. Scale bars equal 100 mm.

and *Macrodelphinus*. In addition, the anterior margin of the nasal at least slightly overhangs the corresponding bony naris, as seen in *Squaloziphius*.

As in *Chilcacetus* and *Macrodelphinus*, the internasal and frontal-nasal sutures are complex, with numerous ridges and grooves. The outline of the nasals is therefore difficult to follow,

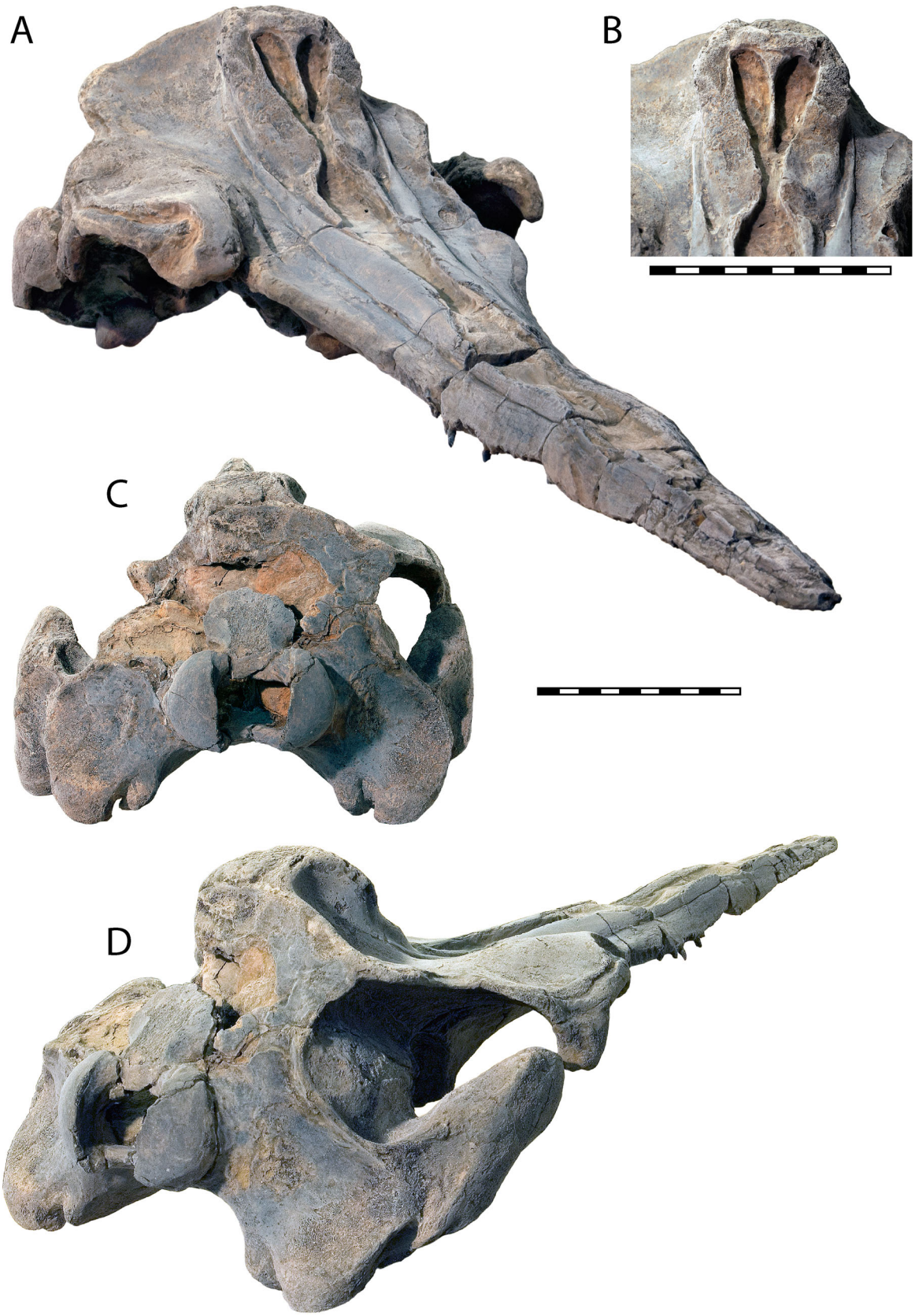

FIGURE 5. Cranium of the holotype of *Yaquinacetus meadi*, gen. et sp. nov., USNM 214705. **A**, right anterodorsolateral view; **B**, anterodorsal view of the vertex; **C**, posterior view; **D**, right posterodorsolateral view. The fossil was lightly coated with sublimed ammonium chloride. Scale bars equal 100 mm.

and here we provide two possible interpretations: one with highly interdigitated sutures and the lateral portion of each nasal posteriorly longer (Fig. 2C) and the other with simpler sutures limiting the nasals and an unidentified medial mass of bone possibly made of the interparietal and/or frontals (Fig. 2B). In both interpretations, the nasals of *Yaquinacetus* are proportionally wider (total width = 35 mm) than in *Squaloziphius*, a condition linked to the less transversely pinched vertex in the former.

Frontal—Depending upon the interpretation of the frontal-nasal suture discussed above, the frontal exposure on the vertex is either much larger than the nasal (as in *Macrodelphinus*) or somewhat larger. The minimum transverse distance between the maxillae across the frontals is proportionally wider than in *Squaloziphius*. The surface of the frontals (possibly joined to the interparietal) on the vertex is slightly longitudinally convex, with deep grooves and ridges (as in, e.g., *Berardius*, *Macrodelphinus*, and *Squalodon*), and slopes gently toward the lower dorsal margin of the supraoccipital shield.

In lateral view (Fig. 4), the preorbital process of the frontal is thick and globular. As in *Squaloziphius*, the postorbital process is robust, moderately vertically elongated, anteroposteriorly wide, and somewhat transversely flattened. This process nearly contacts the zygomatic process of the squamosal.

The frontal groove is long and obliquely directed. The presumed absence of a posterior part of the dorsal lamina of the pterygoid likely emphasizes the length of the groove, ventrally open for a longer distance than in ziphiids. Thin plates of bone on the anterior and posterior walls of the medial portion of the frontal groove possibly correspond to elements of the orbitosphenoid. No trace of a fossa for a postorbital lobe of the pterygoid sinus could be detected on the ventral surface of the frontal, differing from some eurhinodelphinids (e.g., *Schizodelphis* and *Xiphiacetus*).

Vomer—No conspicuous mesorostral ossification of the vomer is observed in the partly prepared, widely open mesorostral groove. The vomer is visible on the ventral surface of the mid-rostrum for more than 100 mm (Fig. 3).

Presphenoid and Cribriform Plate—The high and narrow nasal septum becomes thicker 8 mm anterior to the nasals, making a somewhat abraded triangular surface distinctly lower than the top of the nasal (Figs. 2, 5A, B).

Palatine and Pterygoid—As in *Squaloziphius*, each palatine is widely exposed anterior and anteromedial to the pterygoid (Figs. 3, 6). The two palatines draw to a joint anteromedial point, far anterior to the level of the antorbital notch (Fig. 3B). Parts of the pterygoid-palatine suture are visible anteromedial and anterior to the pterygoid sinus fossa, limiting a short but thick portion of the pterygoid. Although the pterygoid sinus fossa is transversely wide, it ends anteriorly at a level distinctly posterior to the antorbital notch. Even more than in *Squaloziphius*, the fossa is therefore shorter than in stem and crown ziphiids (Lambert et al., 2013). However, the anterior limit of the fossa is 60 mm anterior to the level of the corresponding choana; this is proportionally longer than in eurhinodelphinids, '*Argyrocetus*' *joaquinensis*, *Chilcacetus*, and *Macrodelphinus*. The pterygoid overhangs ventrally a small part of the anterior portion of the pterygoid sinus fossa, but the anterior half of the fossa is floored by the palatine, whereas a thin layer of the pterygoid covers the posterior half. A similar condition is observed in *Squaloziphius* and several other odontocetes (including some ziphiids and delphinids). The hamular process of the pterygoid is possibly incomplete posteroventrally (Fig. 4C), and the presence or absence of solid, finger-like processes as observed in '*Argyrocetus*' *joaquinensis*, *Chilcacetus*, *Simocetus*, and *Squaloziphius* cannot be ascertained. The ventral margin of the pterygoid sinus fossa in the hamular process is shorter ventrally than the posteroventral margin of the basioccipital, a condition less derived than in ziphiids. Due to the poor state of preservation, the posterior extent of the dorsal and lateral laminae of the pterygoid is difficult to describe. Based on the preserved portions, we hypothesize that the lateral lamina of the pterygoid was reduced to a low crest, dorsolaterally barely limiting the broad pterygoid sinus fossa, as also observed in *Chilcacetus* and *Squaloziphius*. The medial lamina of the pterygoid forms the lateral margin of the basioccipital basin for about half its length (Fig. 3B).

Lacrimal and Jugal—Still partly embedded in hardened sediment, the lacrimal and jugal cannot be distinguished from each other (Figs. 2–4). The lacrimojugal complex sends a long lateral extension toward the lateral margin of the antorbital process; the apical part of this element is distinctly anteroposteriorly and dorsoventrally thickened, in a way similar to *Squaloziphius*. As in the latter, in dorsal view, the lacrimal/jugal sends up a thin lamina, wedged between the preorbital process of the frontal and the antorbital process of the maxilla. The slender base of the lost styliform process of the jugal is posterior to the antorbital notch (Fig. 3).

Supraoccipital—Constituting the anterodorsal limit of the supraoccipital shield, the nuchal crest forms a straight line in dorsal view (Fig. 2). In posterodorsal view, the supraoccipital-frontal contact is slightly more anteromedially pointed in *Squaloziphius*. Linked to the more elevated vertex as compared with that in *Squaloziphius*, the partly preserved supraoccipital shield is dorsoventrally higher with a steeper slope in *Yaquinacetus*. Based on the preserved parts, the shield was most likely moderately longitudinally concave (Fig. 5). In dorsal view, the temporal crest does not protrude posteriorly, a feature shared with *Squaloziphius* and many non-platanistoid (sensu Muizon, 1991; Fordyce, 1994) crown odontocetes.

Exoccipital—The occipital condyles, set off on a distinct condylar neck (Fig. 2), are prominent and proportionally small (ratio between the width of the condyles and the bizygomatic width = 0.33). A shallow dorsal condyloid fossa is present. In ventral view, the paroccipital process is robust; its posterolateral portion is excavated by a distinct fossa and the posterior surface bulges posteriorly (Figs. 3, 5). As in *Squaloziphius*, the anterior surface of the paroccipital process is seemingly not excavated, suggesting a shallow or absent posterior sinus (a condition also shared with ziphiids; Fraser and Purves, 1960; Lambert et al., 2013). The posterior lacerate foramen was originally most likely small; it is widely separated from the foramen ovale by an extended bony bridge. The right hypoglossal foramen is visible along the posterodorsal wall of the deep and narrow jugular notch.

Squamosal—The robust zygomatic process of the squamosal is elongated anteriorly. This process is dorsoventrally high, but unlike in platanistids and squalodelphinids, it retains a conspicuously concave ventral margin (Figs. 3, 4, 6). The dorsal portion of the process and the anterior end of the ventral margin (the latter region corresponding to the area of contact with the jugal) are transversely thickened. The mandibular fossa is wide and concave, oriented anteroventrally and slightly medially. As in *Squaloziphius*, the shallow and wide tympanosquamosal recess is only separated from the mandibular fossa by a slightly convex area (Fig. 6A), differing from the abrupt step present in, for example, eurhinodelphinids and ziphiids. Although not extending on the medial flank of the zygomatic process, the recess cuts into the medial surface of the postglenoid process. In its posterior part, the floor of the recess is covered with small crests and grooves. Medially, the recess is defined by a low and anteroposteriorly long crest, just lateral to the squamosal-parietal suture and anteriorly continuous with a longitudinal crest laterally limiting the alisphenoid (see below), as in *Squaloziphius*. On the right side of the holotype of *Yaquinacetus meadi*, a thin and narrow, 18-mm-long bony plate lies, presumably detached, along the anterolateral margin of the in situ tympanic bulla. The position and shape of the plate is strongly reminiscent of the long and narrow vestigial falciform process of ziphiids (and

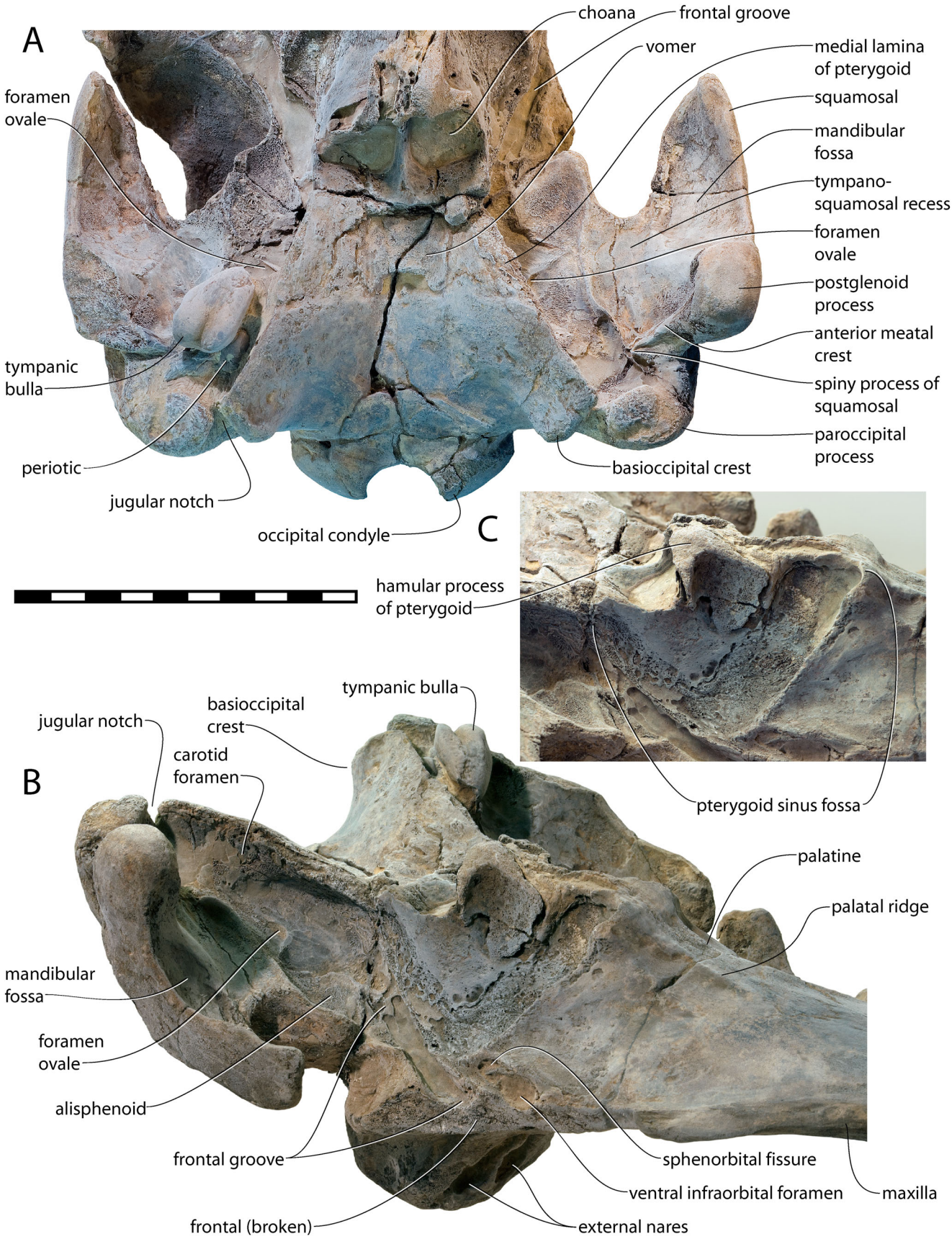

FIGURE 6. Cranium of the holotype of *Yaquinacetus meadi*, gen. et sp. nov., USNM 214705. **A**, ventral view of the basicranium; **B**, basicranium and palate in left anteroventrolateral view; **C**, detail of the palate in left anteroventrolateral view. The fossil was lightly coated with sublimed ammonium chloride. Scale bar equals 100 mm.

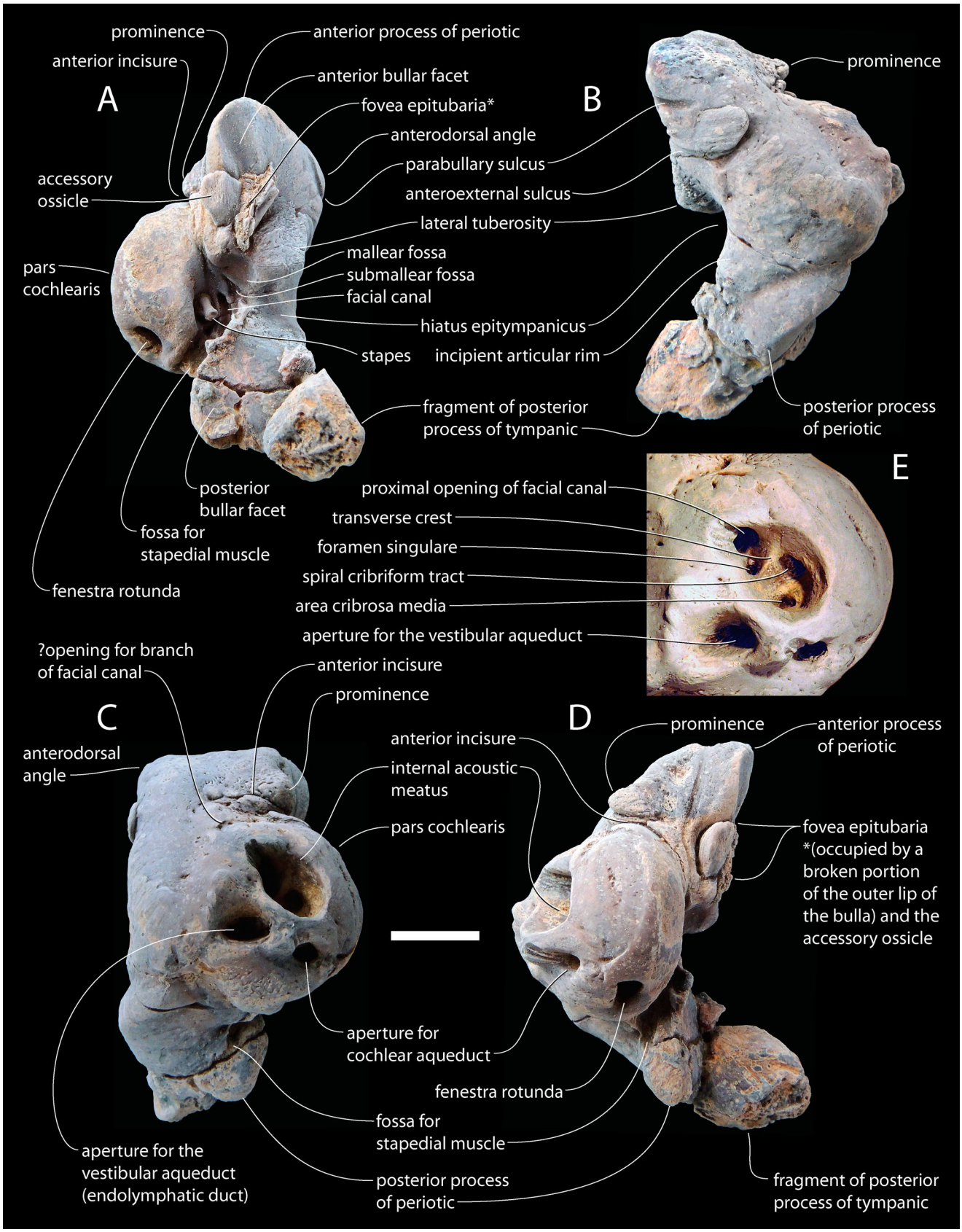

FIGURE 7. Left periotic of the holotype of *Yaquinacetus meadi*, gen. et sp. nov., USNM 214705. **A**, ventral view; **B**, lateral view; **C**, dorsal and slightly medial view; **D**, medial view; **E**, detail of the internal acoustic meatus. The fossil was lightly coated with sublimed ammonium chloride. Scale bar equals 10 mm.

some physeteroids). Additional specimens would be necessary to confirm this interpretation.

In lateral view, the postglenoid process of the squamosal (only complete on the left side of the holotype) is massive (Fig. 6B), with a rounded ventral margin ventrally longer than the post-tympanic region of the squamosal and the ventral margin of the exoccipital, a difference from ziphiids. In ventral view, the apex of the process is transversely thick, much more than in ziphiids (the latter displaying an obliquely flattened postglenoid process). Furthermore, this section of the process is even longer anteroposteriorly than transversely thick, which is a major difference from most other odontocetes (including eurhinodelphinids, *Simocetus*, squalodontids, and *Waipatia*). For all these features, the postglenoid process of *Yaquinacetus* is more similar to that in *Squaloziphius* than any other known odontocete, although this process is unknown in *Chilcacetus*, *Macrodelphinus*, and *Papahu*.

Posterior to the zygomatic and postglenoid processes, the lateral surface of the squamosal is hollowed by two sternocephalicus fossae: the long ventral fossa is obliquely directed and the dorsal fossa is more rounded (Figs. 4, 5). The floor of the squamosal fossa is transversely and longitudinally concave.

Basioccipital—The widely separated and posteriorly diverging basioccipital crests (drawing an angle of 55–60° in ventral view) encompass a vast basioccipital basin; in *Squaloziphius*, the crests diverge more abruptly than in *Yaquinacetus meadi*, as in some ziphiids and physeteroids (Muizon, 1991; Lambert et al., 2013). The ventral portion of the basioccipital crest remains thin for most of its extent, only being swollen in the posteriormost part.

Alisphenoid—As in *Chilcacetus* and *Squaloziphius*, the ventral exposure of the alisphenoid is a wide and concave surface, limited laterally by a well-developed subtemporal crest (Fig. 3). Unlike in most ziphiids, but as in *Squaloziphius*, the dorsal lamina of the pterygoid likely did not cover this part of the alisphenoid. Best seen on the left side, the small, crescent-shaped foramen ovale is anterior to the level of the posterior end of the medial lamina of the pterygoid (Fig. 6). It is followed anterolaterally by a shallow path for mandibular nerve V3, which disappears after 15 mm. No indication for a foramen pseudo-ovale is seen on the squamosal or alisphenoid; the mandibular nerve likely exited the basicranium through soft tissue. Just behind the foramen ovale, a zig-zagging longitudinal suture is tentatively interpreted as the medial margin of the ventral exposure of the parietal. Located at the posterior limit of the pterygoid bone, the opening for the carotid foramen is more posterior than the foramen ovale (Fig. 6B), a condition shared with *Chilcacetus* and *Squaloziphius*, differing from many other odontocetes (including eurhinodelphinids and ziphiids).

Basisphenoid—In both *Squaloziphius* and *Yaquinacetus*, the ventral surface of the basisphenoid is marked by a central circular depression along the posterior margin of the vomer (Figs. 3, 6A), although it is more conspicuously developed in *Squaloziphius*. A roughly similar depression, presumably for the origin of hypaxial musculature, is observed in *Chilcacetus* and several ziphiids, including *Ninoziphius*. Because this character is difficult to detect based on photographs, we cannot exclude that it is more broadly distributed among fossil odontocetes. This depression may be functionally analogous to the tubercle described at the contact with the vomer in *Simocetus* (Fordyce, 2002).

Periotic—The description of the periotic is based primarily on the left one (Fig. 7) because the right periotic is preserved in situ in the basicranium and hidden by the corresponding tympanic (Fig. 6A). The left periotic is well preserved, except for its posterior process; fragments of the posterior process of the tympanic mask the apex of the process.

In ventral view, the anterior process is medially broadened by the presence of a short prominence at the base of its dorsomedial surface. Nevertheless, this widening is less marked than in most ziphiids (except *Messapicetus* and *Ninoziphius*). The lateral surface of the anterior process also displays a swollen aspect in ventral view (as compared, for example, with the transversely narrow process of eurhinodelphinids). This bulging lateral outline of the process only partly corresponds to the laterally swollen process of most ziphiids. Indeed, in *Yaquinacetus*, it is related to a lateral shift of the anterodorsal angle of the process, giving the anterior process a subrectangular outline in lateral view, differing from the condition in *Papahu*. As in *Papahu*, no prominent anterodorsal angle is observed in ziphiids, the latter displaying a more tapering anterior process in lateral/medial view. The prominent anterodorsal angle is surrounded by a sulcus interpreted as the parabullary sulcus (Fig. 7A, B) (sensu Tanaka and Fordyce, 2014). More posteriorly, a second sulcus leaves from the anterolateral margin of the lateral tuberosity in a dorsolateral direction; it is interpreted as the anteroexternal sulcus, also following the description of the periotic of the early platanistoid *Otekaikea* by Tanaka and Fordyce (2014). The anterior bullar facet is transversely concave, making a deep longitudinal groove margined by a crest higher on the medial side than on the lateral side. The small and elongated accessory ossicle of the tympanic and a fragment of the outer lip are attached in the fovea epitubaria (Fig. 7A). A larger ossicle, in a correspondingly wider fovea, is observed in physeteroids and in some ziphiids. A narrow longitudinal groove between the accessory ossicle and the pars cochlearis probably corresponds to the origin of the tensor tympani muscle (see Luo and Marsh, 1996). Although prominent, the lateral tuberosity is shorter laterally than in ziphiids, not reaching a level beyond the lateral outline of the periotic. The shallow mallear fossa faces posteroventromedially. Posterior to the mallear fossa and anterolateral to the distal opening of the facial canal, another transversely narrow fossa is identified as the submallear fossa (sensu Tanaka and Fordyce, 2016); a similar fossa is present in several archaic platanistoids, including *Waipatia* (Tanaka and Fordyce, 2016), and, to a varying degree, in eurhinodelphinids (e.g., *Eurhinodelphis cocheteuxi* IRSNB M.1856) and ziphiids (e.g., *Mesoplodon bidens* IRSNB 16232). The hiatus epitympanicus is deep and opens broadly ventrolaterally.

In ventral view, the pars cochlearis is proportionally mediolaterally low and anteroposteriorly long, with a rounded outline. The ventral surface of the pars cochlearis is roughly flat, with a slightly concave area anteromedial to the fenestra ovalis, medially margined by a low longitudinal crest. The large fenestra rotunda has a semicircular outline, without any groove extending toward the aperture for the cochlear aqueduct. The medium-sized, circular aperture for the cochlear aqueduct is closer to the internal acoustic meatus than to the larger and anteroposteriorly flattened aperture for the endolymphatic duct (Fig. 7C, D). The latter aperture is dorsolateral to the lateral margin of the spiral cribriform tract (Fig. 7E), unlike in ziphiids. A cochlear spine is located ventral to this aperture, being less developed than in the holotype of *Ninoziphius platyrostris* (Muizon, 1984). Another short protuberance is anterolateral to the aperture. The internal acoustic meatus is oval, lacking any elevated ventral rim. In the meatus, the circular proximal opening of the facial canal is slightly anterior to the spiral cribriform tract, and is separated from the latter by a low transverse crest (Fig. 7E). The foramen singulare is located on the anterior wall of the crest, thus closer to the opening for the facial canal. A supplementary tiny opening pierces the pars cochlearis just before the contact with the anterior process; similarly observed in eurhinodelphinids and *Waipatia*; it may have conducted a branch of the facial canal or the greater petrosal nerve (Fordyce, 1994; Lambert, 2005). The body of the periotic (tegmen tympani) barely projects dorsal to the internal acoustic meatus and aperture for the endolymphatic duct. The dorsal surface of the bone is flat to convex.

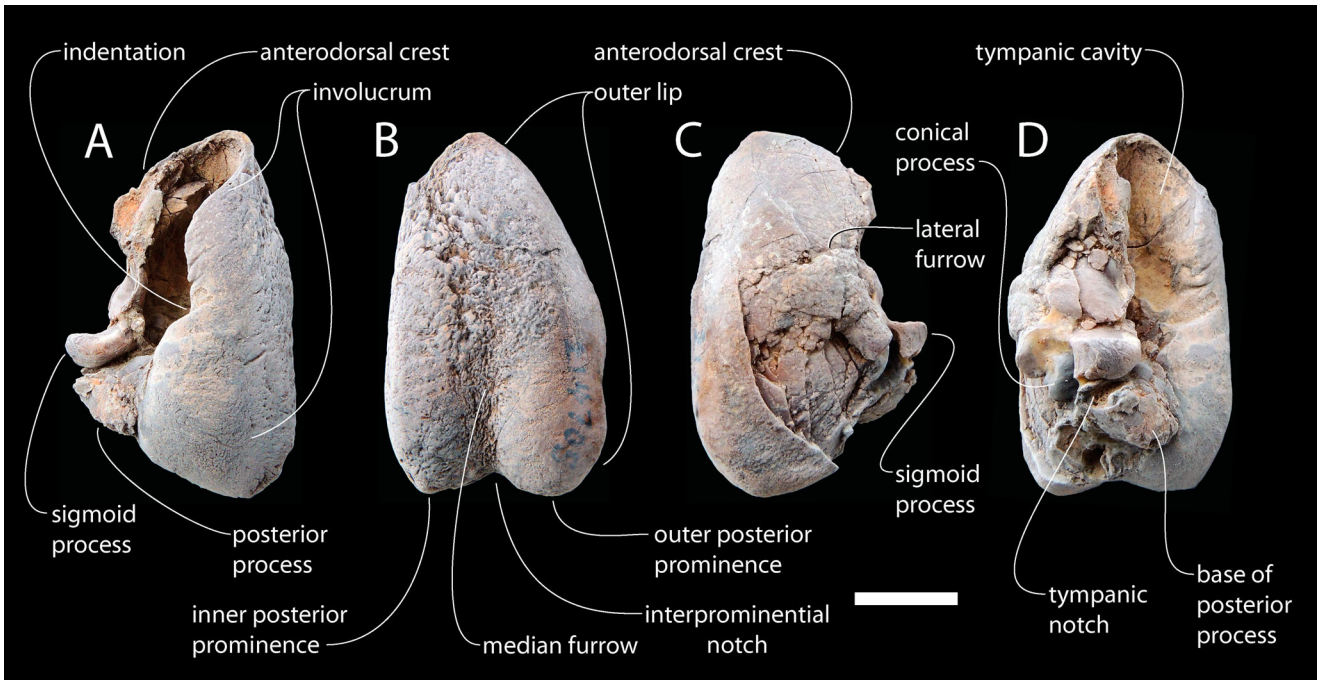

FIGURE 8. Left tympanic of the holotype of *Yaquinacetus meadi*, gen. et sp. nov., USNM 214705. **A**, medial view; **B**, ventral view; **C**, lateral view; **D**, dorsal view. The fossil was lightly coated with sublimed ammonium chloride. Scale bar equals 10 mm.

The distal opening of the facial canal is anterior to the level of the nearly circular fenestra ovalis (Fig. 7A). The facial sulcus is short, ending before the posterodorsal margin of the stapedial muscle fossa. The latter only extends for a short distance along the medial surface of the posterior process. Medial to the stapedial muscle fossa is a dorsoventrally elongated depressed surface at the contact between the pars cochlearis and the posterior process; this shallow concave region may correspond to the stylomastoid fossa (sensu Geisler and Luo, 1996).

As in some eurhinodelphinids, *Waipatia*, and even some ziphiids, a low, incipient articular rim is observed anterolateral to the posterior bullar facet (Fig. 7B), much lower than in platanistids and squalodelphinids. Partly obscured by remains of the posterior process of the tympanic, the posterior bullar facet is smooth along the exposed surface, slightly longitudinally concave, and nearly transversely flat, with only a slightly ventromedially curved facial crest. The slight posteroventrolateral curve is still more pronounced than in platanistids, squalodelphinids, and squalodontids. The absence of any indication of the fossa incudis at the anterior tip of the posterior bullar facet may be due to damage. The dorsolateral surface of the posterior process is keeled (Fig. 7B, C), probably a plesiomorphic condition much less frequently observed in ziphiids than in eurhinodelphinids and platanistoids (sensu Muizon, 1991).

Tympanic Bulla—The left tympanic bulla is detached from the cranium (Fig. 8), whereas the right is preserved in situ (Fig. 3, 6A). Most of the elements described here are based on the left tympanic, of which only part of the outer lip and the posterior process are damaged. Although a short part of the thin anterior margin could be missing, no solid anterior spine was present in *Yaquinacetus*. The median furrow is relatively short, ending at mid-length of the ventral surface; this is somewhat shorter than in eurhinodelphinids, *Macrodelphinus*, and the stem ziphiids *Messapicetus* and *Ninoziphius*, but still much more developed than in *Eoplatanista*. Although the inner posterior prominence is narrower and more ventrally keeled compared with the outer prominence, the difference is less marked than in *Messapicetus* and *Ninoziphius*. The inner prominence is slightly posteriorly shorter than the outer prominence. In lateral view, an abrupt indentation marks the dorsal margin of the involucrum, as in eoplatanistids, eurhinodelphinids, *Chilcacetus*, and ziphiids. The posterior part of the involucrum is high, differing from the dorsoventrally flattened condition in ziphiids. The sigmoid process is only partly preserved; its posterior margin was transversely oriented, lacking the posterior projection of the ventrolateral part of this margin seen in most ziphiids (except *Ninoziphius*). The ventral part of a narrow lateral furrow is visible. In posterior view, an elliptical foramen with a transverse width of 1.6 mm is observed.

On the basicranium, as in *Squaloziphius*, no indication of an enlarged posterior process of the tympanic is found; this is potentially another difference from ziphiids (and physeteroids), which possess a large posterior process of the tympanic, partly fused to the squamosal/exoccipital (Muizon, 1991; Lambert et al., 2013).

Malleus—The posteromedial view of this ear ossicle (Fig. 9F) reveals a relatively shortened tubercule compared with the head (bearing the articular facets with the incus); the tubercule is much shorter than the articular facets, a condition differing from most known odontocetes, except eurhinodelphinids, physeteroids, and ziphiids (Muizon, 1985; Lambert, 2005; Bianucci et al., 2010). The tubercule is longer and more robust than in extant ziphiids and physeteroids; less pointed than in the stem ziphiid *Messapicetus*, it is more similar to the tubercule in eurhinodelphinids (e.g., *Eurhinodelphis cocheteuxi*). The muscular process (for the insertion of the tensor tympani muscle) is only slightly higher or roughly at the same level as the manubrium (for the insertion of the tympanic ligament), whereas the manubrium is higher in *Eurhinodelphis cocheteuxi* and *Schizodelphis morckhoviensis*.

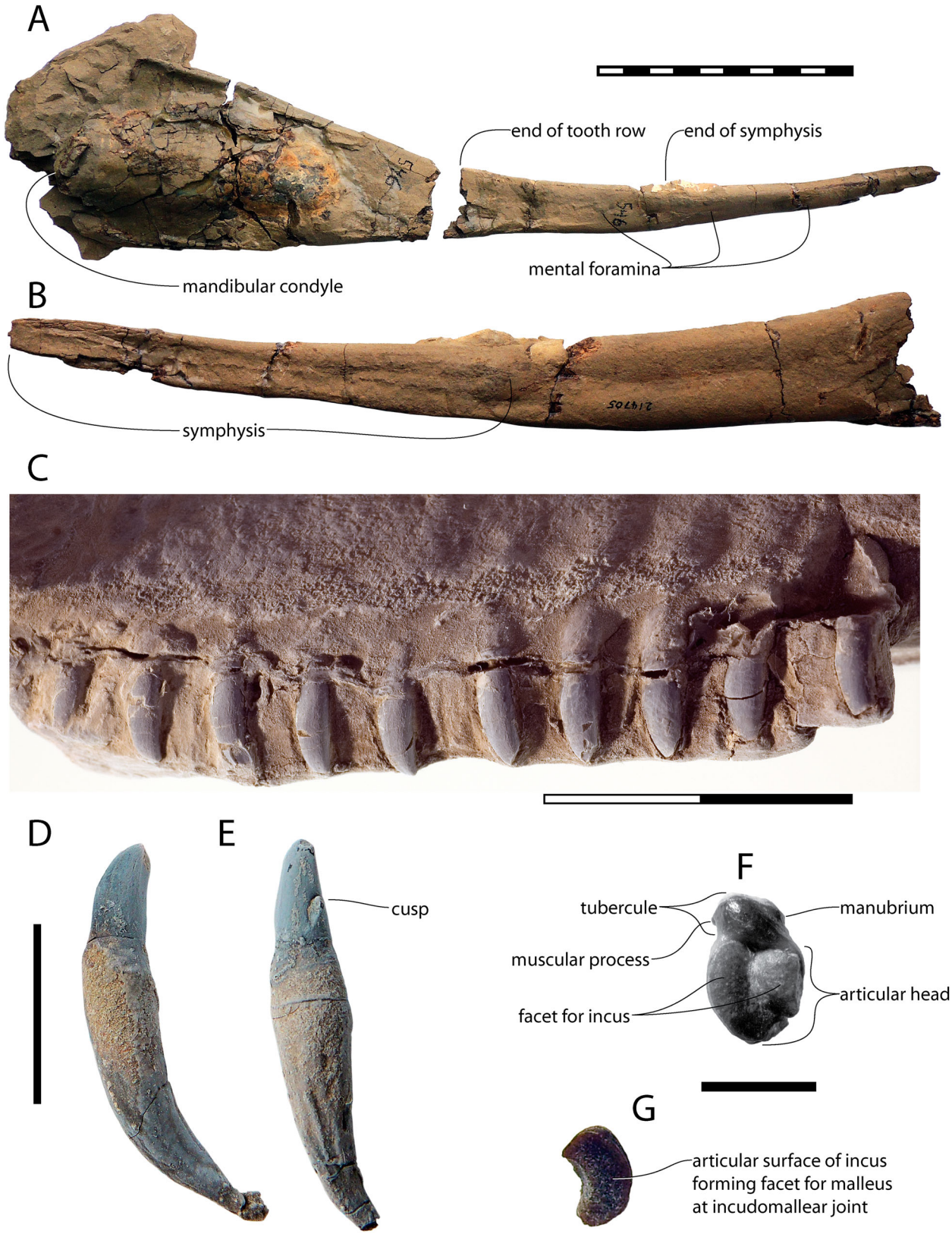

FIGURE 9. Holotype of *Yaquinacetus meadi*, gen. et sp. nov., USNM 214705. **A**, right hemimandible in lateral view; **B**, anterior portion of right hemimandible in medial view, lacking the postalveolar region; **C**, detail of in situ right posterior maxillary teeth in lateral view; **D**–**E**, detached teeth (with the presence of an accessory denticle, tooth in **E** presumably from the posterior end of the upper or lower tooth row); **F**, left malleus in posteromedial view; **G**, fragment of the left incus in anterolateral view. The mandible and teeth were lightly coated with sublimed ammonium chloride. Scale bars equal 100 mm (**A**–**B**), 20 mm (**C**), 10 mm (**D**), and 5 mm (**F**–**G**).

Incus—Only a small part of the left incus is preserved (Fig. 9G); this is the 3.8-mm-high articulation facet, perfectly matching the largest facet on the malleus.

Stapes—In situ in the fenestra ovalis (Fig. 7A), the stapes has a roughly circular stapedial footplate, differing from the more elliptical footplate in *Physeter* and some delphinoids (Lambert et al., 2009). Although much reduced as compared with that in the basilosaurid *Dorudon* (Uhen, 2004), the tiny intercrural aperture (stapedial foramen) may have remained open.

Mandible—The right hemimandible is nearly complete (Fig. 9A); the fragile medial surface of its ramus is only partly prepared, and most of the alveoli are filled with hardened sediment, precluding any precise estimate of the lower tooth count. The ventral and dorsal margins of the slender body of the mandible both rise slightly anterodorsally. The nonankylosed mandibular symphysis (thus differing from eurhinodelphinids, some ziphiids, and many platanistoids) is elongated, making up about 30% of the total length (Fig. 9B). The posterior elevation of the moderately high coronoid process is progressive and regular, without any indication of a precoronoid crest (the latter is observed in most ziphiids and some delphinoids). The angular process is well defined, with the ventral margin at some distance from the ventral margin of the mandibular condyle. The lateral surface of the mandible lacks any lateral groove; three mental foramina are visible along the body (Fig. 9A). In dorsal view, the body remains thin for the whole length of the alveolar groove, not leaving any space for an enlarged apical or subapical mandibular tusk as observed in all fossil ziphiids for which the mandible is preserved.

Teeth—The crown of the small, single-rooted maxillary and mandibular teeth (some of them preserved in situ [Fig. 9C] and others detached [Fig. 9D, E]) is simple, conical, and pointed; apart from a small accessory denticle identified on the crown of a detached tooth (Fig. 9E), no ornamentation is observed. The length of the preserved crowns reaches 8 mm, with a maximum diameter ranging from 2.3 to 2.8 mm. In some teeth, a small portion of the crown apex is truncated, due to either wear or breakage. No other indications of wear are noted along available surfaces. Partially worn maxillary alveoli and detached teeth show long and slender dental roots (lacking the swollen aspect of fossil and extant adult ziphiid dental roots; Muizon, 1984; Bianucci et al., 2010), with a posterodorsally directed proximal portion.

Vertebrae—Eighteen vertebrae were found associated with the cranium of the holotype. Because these vertebrae are only partially preserved (most transverse processes and neural spines are lost) and partly embedded in hardened sediment (with five of them forming a single block), only a few measurements (Table 2) and observations can be provided here. Based on the presence of hemal processes, nine vertebrae were identified as caudals. Most, if not all, other vertebrae are lumbars. Because the exact position along the axial column of these vertebrae is unknown, they were lettered from front to back beginning at 'A' and ending with 'M' (Table 2). The transverse processes of lumbar D curve distinctly ventrolaterally. The centrum of caudal M is higher and wider than long, and its anterior surface is convex; it is thus tentatively identified as the ball vertebra, marking the junction between the peduncle and the fluke (Fish et al., 2006).

PHYLOGENY

To investigate the phylogenetic relationships of *Yaquinacetus meadi*, we added the holotype (USNM 214705) to the morphological matrix of the analysis by Lambert et al. (2018; Supplementary Data 1), together with the other archaic homodont odontocetes '*Argyrocetus*' *bakersfieldensis*, *Chilcacetus cavirhinus*, and *Macrodelphinus kelloggi*. *Chilcacetus cavirhinus* and *M. kelloggi* were coded based on direct observations of the type material, whereas '*A.*' *bakersfieldensis* was coded using a cast of the upper part of the holotype cranium at IRSNB and data from Wilson (1935). Besides these additions, we modified several codings for *Squaloziphius emlongi*, following direct observation of the holotype. Finally, due to their high volatility in preliminary analyses and their remote relationships with the clades targeted in this work, we removed from the taxon list a series of poorly known delphinidans lacking a well-preserved basicranium and, for most of them, the ear bones. These include the inioids *Auroracetus bakerae*, *Ischyrorhynchus vanbenedeni*, *Meherrinia isoni*, *Protophocaena minima*, and *Stenasodelphis russellae*, the early delphinidans *Lophocetus calvertensis* and *Pithanodelphis cornutus*, as well as the unpublished specimen ChM PV4802, for which we could not check the codings. The resulting total number of taxa is 102. The parsimony analyses were performed using PAUP version 4.0 (Swofford, 2001), with *Bos taurus*, *Hippopotamus amphibius*, and *Sus scrofa* as outgroups. A constraint tree obtained from Bayesian analysis of molecular data (nuclear and mitochondrial; McGowen et al., 2009, 2011; Geisler et al., 2011; Supplementary Data 2) was first used as a backbone to force relationships among extant cetaceans, as in Lambert et al. (2017, 2018). A total of 147 multistate characters

TABLE 2. Measurements (in mm) of the vertebrae of the holotype of *Yaquinacetus meadi*, gen. et sp. nov., USNM 214705, including four lumbars and nine caudals.

Element	Centrum length	Centrum anterior height	Centrum anterior width	Centrum posterior height	Centrum posterior width	Maximum width
Lumbars						
A	67	—	—	—	—	—
B	70	—	—	53	54	—
C	66	—	—	52	56	—
D	e70	—	—	e58	65	+183
Caudals						
E	e67	—	—	e61	71	—
F	72	—	—	63	63	—
G	e63	e64	71	—	—	—
H	67	e60	60	—	—	—
I	e69	—	—	—	60	—
J	67	60	64	—	—	—
K	e62	—	—	e60	56	—
L	57	e56	e56	e50	e50	—
M	38	e55	e55	e44	e44	—

e, estimate; +, not complete; —, no data.

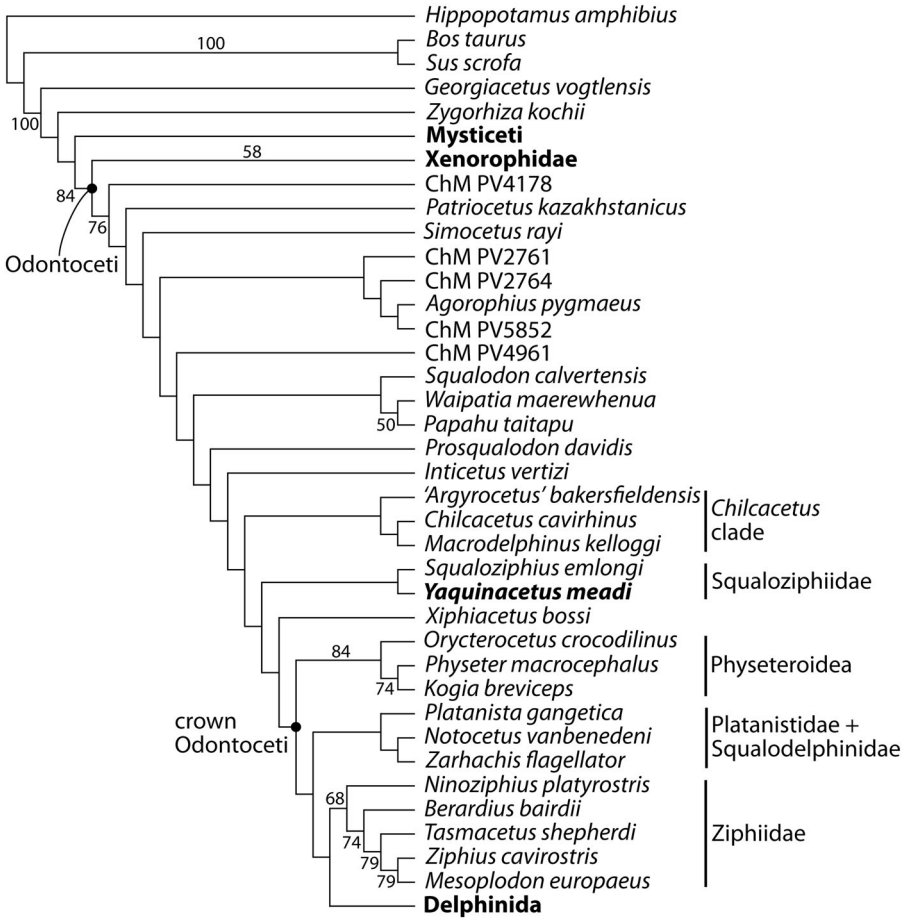

FIGURE 10. Most parsimonious tree resulting from the cladistic analysis (heuristic search) of a morphological matrix modified from Lambert et al. (2017), with a molecular constraint applied as a backbone. This tree shows the relationships of *Yaquinacetus meadi*, gen. et sp. nov., with other archaic homodont odontocetes. Several clades (Mysticeti, Xenorophidae, and Delphinida) were collapsed for clarity. Numbers indicate bootstrap support values. Complete tree can be found in Supplementary Data 3 (Fig. S1).

were ordered, following the criteria used by Geisler et al. (2011). All ordered multistate characters were scaled in such a way that the minimum length for each is 1 step, as for binary characters (see Geisler et al., 2011). The heuristic search was performed with simple taxon addition, a tree-bisection-reconnection algorithm, and ACCTRAN optimization. This analysis resulted in a single most parsimonious tree, with tree length 2054 steps, consistency index (CI) 0.16, and retention index (RI) 0.56 (Fig. 10; Supplementary Data 3, Fig. S1).

First, it should be noted that many of the proposed relationships are poorly supported, with bootstrap values often lower than 50. The addition of other taxa and the use of different settings will most likely lead to different topologies, as observed in previous analyses with earlier versions of this matrix (Geisler et al., 2011, 2014; |Lambert et al., 2017, 2018). The main results are as follows. *Papahu taitapu*, *Squalodon calvertensis*, and *Waipatia maerewhenua* are not closely related to platanistids and squalodelphinids, forming a clade of stem odontocetes branching before *Prosqualodon davidis.* The exclusion of these taxa (or some of them) from the superfamily Platanistoidea was previously found in several analyses (Vélez-Juarbe, 2017; some of the trees in Lambert et al., 2018, and Tanaka and Fordyce, 2016, 2017). Following *P. davidis*, the next stem odontocete branch leads to the recently described heterodont odontocete *Inticetus vertizi*, previously interpreted as either an early branching platanistoid or a late branching stem odontocete (Lambert et al., 2018). The next clade of stem odontocetes includes the North and South Pacific homodont taxa '*Argyrocetus*' *bakersfieldensis*, *Chilcacetus cavirhinus*, and *Macrodelphinus kelloggi*, already previously grouped (with a different matrix), together with '*Argyrocetus' joaquinensis* and *Argyrocetus patagonicus*, in the *Chilcacetus* clade (Lambert et al., 2015). *Squaloziphius emlongi* is recovered here as a stem odontocete, as in several earlier analyses (Geisler et al., 2011, 2014; Godfrey et al., 2016; Vélez-Juarbe, 2017). *Squaloziphius emlongi* is thus not closely related to ziphiids, and, as proposed above based on a series of shared cranial features, is sister group to the newly described *Yaquinacetus meadi*, a result that supports the proposal to define a family Squaloziphiidae including these two roughly contemporaneous North Pacific taxa. The relatively low support value (bootstrap <50) obtained for this sister-group relationship is at least partly explained by the absence (or the different formulation) of some of the most striking synapomorphies of this clade in the character list of the cladistic analysis (the transversely wide dorsal opening of the mesorostral groove at base of rostrum, followed posteriorly by an abrupt narrowing, and the apex of the postglenoid process being anteroposteriorly longer than transversely thick). The next and last stem odontocete branch is the one of the eurhinodelphinid *Xiphiacetus bossi*, an interesting result considering that close relationships of *S. emlongi* with eurhinodelphinids have been proposed earlier (Fordyce and Barnes, 1994; Fordyce, 2002).

If the molecular constraint is removed, the clade *Squaloziphius emlongi* + *Yaquinacetus meadi* is retained (Supplementary Data 3, Fig. S2), but inside crown Odontoceti, being more crownward than platanistoids, and sister group to a clade including

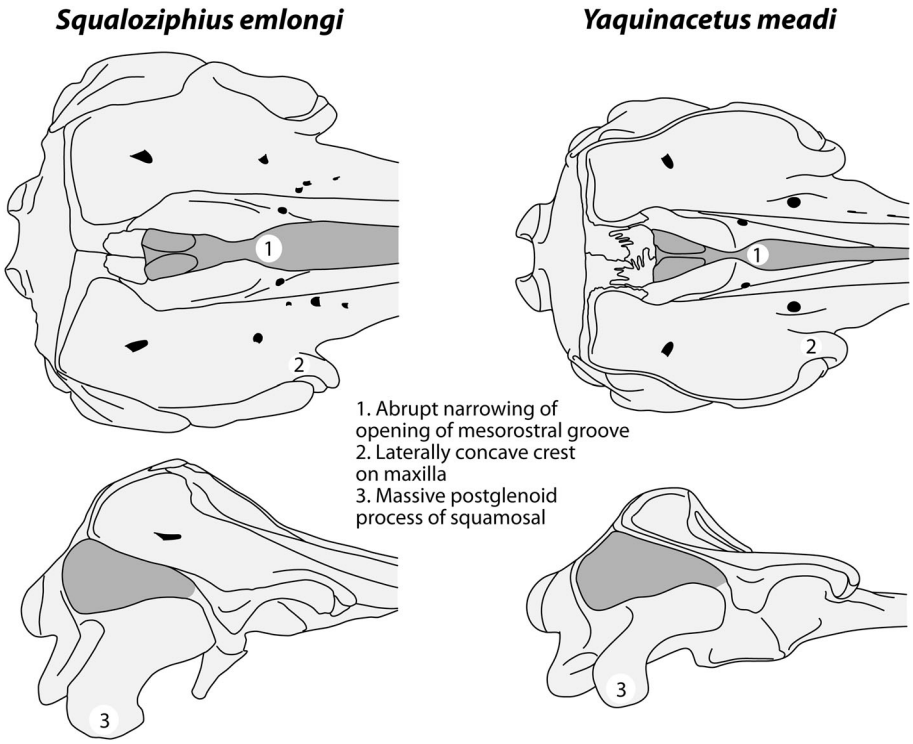

FIGURE 11. Schematic line drawings comparing the neurocranium of the two currently recognized members of the family Squaloziphiidae, fam. nov.: *Squaloziphius emlongi* and *Yaquinacetus meadi*, gen. et sp. nov., in dorsal and right lateral views. Numbers indicate several shared morphological traits. Both neurocrania scaled at the same anteroposterior length (from occipital condyles to antorbital processes). Dark gray shading for dorsal opening of mesorostral groove, bony nares, and temporal fossa; black for main foramina (premaxillary foramina and dorsal infraorbital foramina).

Xiphiacetus bossi and the *Chilcacetus* clade. In this case, physeteroids and ziphiids form a clade branching just after this group of archaic homodont odontocetes.

DISCUSSION

Based on a partial skeleton from latest Oligocene–early Miocene deposits of Oregon, including a finely preserved skull, the new genus and species *Yaquinacetus meadi* differs from all other archaic homodont odontocetes described so far. It shares several similarities with *Squaloziphius emlongi*, from the early Miocene of Washington State, including transversely wide dorsal opening of the mesorostral groove at base of rostrum, followed posteriorly by an abrupt narrowing toward anterior margin of bony nares; thickened lateral margin of the maxilla in the antorbital region making a long and laterally concave crest; and a massive postglenoid process of the squamosal, being longer ventrally than the posttympanic process and exoccipital, and anteroposteriorly longer than transversely thick (Fig. 11). These shared characters suggest that these two geographically and temporally close species belong to the same clade, a hypothesis confirmed by two phylogenetic analyses, with and without a molecular constraint, and leading to the definition of the family Squaloziphiidae (fam. nov.). Indeed, the subfamily Squaloziphiinae was previously referred to the family Ziphiidae (Muizon, 1991), but the description in *Y. meadi* of parts of the skull unknown in the holotype of *S. emlongi* allowed for the detection of new differences from Ziphiidae (aperture for the endolymphatic duct being dorsolateral to the dorsal margin of the spiral cribriform tract on the periotic; prominent anterodorsal angle of the periotic being laterally shifted compared with anterior tip of anterior process; tubercule of the malleus being less reduced than in ziphiids; and enlarged alveoli for mandibular tusks being absent), in addition to differences already noted in *S. emlongi* and confirmed in *Y. meadi* (pterygoid sinus fossa not reaching anteriorly the level of the antorbital notch and distant ventrally from the ventralmost level of the basicranium; probable absence of an enlarged posterior process of the tympanic bulla).

Another clade of early Miocene homodont odontocetes from the Pacific is identified (*Chilcacetus* clade), either also including the eurhinodelphinid *Xiphiacetus bossi* and being sister group to Squaloziphiidae (analysis without molecular constraint) or being stemward to the latter (with molecular constraint). These two clades (*Chilcacetus* clade and Squaloziphiidae) are either among the last stem odontocetes to branch or crownward to Platanistoidea among crown Odontoceti.

With *Squaloziphius emlongi* and *Yaquinacetus meadi* being recovered as only distantly related to ziphiids in our phylogenetic analysis, the presence in both Squaloziphiidae and Ziphiidae of well-defined premaxillary crests along the vertex is interpreted as resulting from convergent evolution, an interpretation that was similarly given for the facial region of the ziphiid-like Pliocene delphinid *Australodelphis mirus*, which bears an elevated and narrow vertex with a lateral expansion of the premaxillae (Fordyce et al., 2002). Being associated with a toothless upper jaw, the similarities shared by the latter with ziphiids lead the authors to suggest that this extinct Antarctic dolphin was a suction feeder, possibly preying upon squid. Because *Y. meadi* retains complete upper and lower dentition (unknown in *S. emlongi*), and despite a proportionally low temporal fossa in the two North Pacific species and a relatively slender rostrum in *Y. meadi*, such a degree of specialization toward suction feeding cannot be proposed here; teeth were still available, at least for prey capture, in *Y. meadi*. Several extinct ziphiid species, and even one extant species, retain a functional set of upper and lower teeth (Bianucci et al., 2016), indicating that, in that family too, suction feeding is not strongly correlated with this unusual development of the premaxillae on the vertex. Located in close proximity to the area responsible for the

production of echolocation sounds (see Heyning, 1989; Cranford et al., 1996), these changes in the topology of the facial area evolving convergently in several groups of homodont odontocetes thus may rather be linked to a currently unknown specialization of the sonar system.

Finally, the description of the new genus and species *Yaquinacetus meadi* and the resulting phylogenetic relationships confirm that the Pacific, and more specifically the northeastern Pacific, was a center of diversification for several groups of archaic homodont odontocetes during the late Oligocene and early Miocene (see Boersma and Pyenson, 2016; Boersma et al., 2017; Peredo et al., 2018).

ACKNOWLEDGMENTS

We thank L. G. Barnes and V. R. Rhue (LACM), D. J. Bohaska, J. G. Mead, C. W. Potter, and N. D. Pyenson (USNM), C. de Muizon and C. Lefèvre (MNHN), S. Bruaux and G. Lenglet (IRSNB), and R. Salas-Gismondi and R. Varas-Malca (MUSM) for generously providing access to the collections of both fossil and extant odontocetes in their care. J. Pojeta (USNM) allowed the use of his laboratory to whiten the skull of the holotype of *Yaquinacetus meadi* with ammonium chloride. We thank J. G. Mead for constructive discussions during preliminary steps of this study, C. de Muizon for discussions on the relationships of *Squaloziphius emlongi*, D. J. Bohaska for kindly providing field notes of D. R. Emlong, and J. H. Geisler (NYIT) for providing matrix and constraint tree files compatible with PAUP. Constructive comments from the reviewers A. T. Boersma and M. D. Nelson and the editor M. Borths improved the quality of this work. This publication was made possible with funding from the Citizens of Calvert County, Maryland, and the Clarissa and Lincoln Dryden Endowment for Paleontology at the Calvert Marine Museum.

ORCID

Olivier Lambert http://orcid.org/0000-0003-0740-5791

LITERATURE CITED

Addicott, W. A., 1976. Neogene molluscan stages of Oregon and Washington; pp. 95–116 in A. E. Fritsche, H. Ter Best Jr., and W. W. Wornardt (eds.), The Neogene Symposium. Society of Economic Paleontologists and Mineralogists, San Francisco, California, April 1976.

Aguirre-Fernández, G., and R. E. Fordyce. 2014. *Papahu taitapu*, gen. et sp. nov., an early Miocene stem odontocete (Cetacea) from New Zealand. Journal of Vertebrate Paleontology 34:195–210.

Barnes, L. G. 2006. A phylogenetic analysis of the superfamily Platanistoidea (Mammalia, Cetacea, Odontoceti). Beiträge zur Paläontologie 30:25–42.

Berta, A. 1991. New *Enaliarctos* (Pinnipedimorpha) from the Oligocene and Miocene of Oregon and role of "enaliarctids" in pinniped phylogeny. Smithsonian Contributions to Paleobiology 69:1–33.

Berta, A. 1994. A new species of phocoid pinniped *Pinnarctidion* from the early Miocene of Oregon. Journal of Vertebrate Paleontology 14:405–413.

Bianucci, G., O. Lambert, and K. Post. 2010. High concentration of long-snouted beaked whales (genus *Messapicetus*) from the Miocene of Peru. Palaeontology 53:1077–1098.

Bianucci, G., C. Di Celma, M. Urbina, and O. Lambert. 2016. New beaked whales from the late Miocene of Peru and evidence for convergent evolution in stem and crown Ziphiidae (Cetacea, Odontoceti). PeerJ 4:e2479.

Boersma, A. T., and N. D. Pyenson. 2016. *Arktocara yakataga*, a new fossil odontocete (Mammalia, Cetacea) from the Oligocene of Alaska and the antiquity of Platanistoidea. PeerJ 4:e2321.

Boersma, A. T., M. R. McCurry, and N. D. Pyenson. 2017. A new fossil dolphin *Dilophodelphis fordycei* provides insight into the evolution of supraorbital crests in Platanistoidea (Mammalia, Cetacea). Royal Society Open Science 4:170022.

Brinkman, D. B. 2009. A sea turtle skull (Cheloniidae: Carettini) from the lower Miocene Nye Formation of Oregon, U. S. A. Paludicola 7 (2):39–46.

Brisson, M. J. 1762. Regnum animale in classes IX distributum, sive synopsis methodica sistens generalum Animalium distributionem in classes IX, & duarum primarum classium, Quadrupedum scilicet & Cetaceorum, particularem divisionem in ordines, sections, genera & species. T. Haak, Paris, 296 pp.

Cranford, T. W., M. Amundin, and K. S. Norris. 1996. Functional morphology and homology in the Odontocete nasal complex: implications for sound generation. Journal of Morphology 228:223–285.

Dawson, S. D. 1996. A new kentriodontid dolphin (Cetacea; Delphinoidea) from the Middle Miocene Choptank Formation, Maryland. Journal of Vertebrate Paleontology 16:135–140.

Domning, D. P., and C. E. Ray. 1986. The earliest sirenian (Mammalia: Dugongidae) from the eastern Pacific Ocean. Marine Mammal Science 2:263–276.

Fish, F. E., M. K. Nusbaum, J. T. Beneski, and D. R. Ketten. 2006. Passive cambering and flexible propulsors: cetacean flukes. Bioinspiration & Biomimetics 1:S42–S48.

Flower, W. H. 1867. Description of the skeleton of *Inia geoffrensis* and the skull of *Pontoporia blainvillii*, with remarks on the systematic position of these animals in the Order Cetacea. Transactions of the Zoological Society of London 6:87–116.

Fordyce, E. R. 1994. *Waipatia maerewhenua*, new genus and new species (Waipatiidae, New Family), an archaic Late Oligocene dolphin (Cetacea: Odontoceti: Platanistoidea) from New Zealand. Proceedings of the San Diego Society of Natural History 29:147–178.

Fordyce, R. E. 2002. *Simocetus rayi* (Odontoceti: Simocetidae) (new species, new genus, new family), a bizarre new archaic Oligocene dolphin from the eastern North Pacific. Smithsonian Contributions to Paleobiology 93:185–222.

Fordyce, R. E., and L. G. Barnes. 1994. The evolutionary history of whales and dolphins. Annual Review of Earth and Planetary Science 22:419–455.

Fordyce, R. E., and C. de Muizon. 2001. Evolutionary history of cetaceans: a review; pp. 169–233 in J.-M. Mazin and V. de Buffrénil (eds.), Secondary Adaptation of Tetrapods to Life in Water. Verlag Dr. Friedrich Pfeil, Munich, Germany.

Fordyce, R. E., P. G. Quilty, and J. Daniels. 2002. *Australodelphis mirus*, a bizarre new toothless ziphiid-like fossil dolphin (Cetacea: Delphinidae) from the Pliocene of Vestfold Hills, East Antarctica. Antarctic Science 14:37–54.

Fraser, F. C., and P. E. Purves. 1960. Hearing in cetaceans: evolution of the accessory air sacs and the structure of the outer and middle ear in recent cetaceans. Bulletin of the British Museum (Natural History), Zoology 7:1–140.

Gatesy, J., J. H. Geisler, J. Chang, C. Buell, A. Berta, R. W. Meredith, M. S. Springer, and M. R. McGowen. 2013. A phylogenetic blueprint for a modern whale. Molecular Phylogenetics and Evolution 66:479–506.

Geisler, J. H., and Z.-X. Luo. 1996. The petrosal and inner ear of *Herpetocetus* sp. (Mammalia: Cetacea) and their implications for the phylogeny and hearing of archaic mysticetes. Journal of Paleontology 70:1045–1066.

Geisler, J. H., and A. E. Sanders. 2003. Morphological evidence for the phylogeny of Cetacea. Journal of Mammalian Evolution 10:23–129.

Geisler, J. H., M. W. Colbert, and J. L. Carew. 2014. A new fossil species supports an early origin for toothed whale echolocation. Nature 508:383–386.

Geisler, J. H., S. J. Godfrey, and O. Lambert. 2012. A new genus and species of late Miocene inioid (Cetacea: Odontoceti) from the Meherrin River, North Carolina, U.S.A. Journal of Vertebrate Paleontology 32:198–211.

Geisler, J. H., M. R. McGowen, G. Yang, and J. Gatesy. 2011. A supermatrix analysis of genomic, morphological, and paleontological data for crown Cetacea. BMC Evolutionary Biology 11:112.

Godfrey, S. J., M. D. Uhen, J. E. Osborne, and L. E. Edwards. 2016. A new specimen of *Agorophius pygmaeus* (Agorophiidae, Odontoceti, Cetacea) from the early Oligocene Ashley Formation of South Carolina, USA. Journal of Paleontology 90:154–169.

Heyning, J. E. 1989. Comparative facial anatomy of beaked whales (Ziphiidae) and a systematic revision among the families of extant

Odontoceti. Contributions in Science, Natural History Museum of Los Angeles County 405:1–64.
Kimura, T., and L. G. Barnes. 2016. New Miocene fossil Allodelphinidae (Cetacea, Odontoceti, Platanistoidea) from the North Pacific Ocean. Bulletin of the Gunma Museum of Natural History 20:1–58.
Lambert, O. 2005. Phylogenetic affinities of the long-snouted dolphin *Eurhinodelphis* (Cetacea, Odontoceti) from the Miocene of Antwerp. Palaeontology 48:653–679.
Lambert, O., and S. Louwye. 2006. *Archaeoziphius microglenoideus*, a new primitive beaked whale (Mammalia, Cetacea, Odontoceti) from the Middle Miocene of Belgium. Journal of Vertebrate Paleontology 26:182–191.
Lambert, O., G. Bianucci, and K. Post. 2009. A new beaked whale (Odontoceti, Ziphiidae) from the middle Miocene of Peru. Journal of Vertebrate Paleontology 29:910–922.
Lambert, O., C. de Muizon, and G. Bianucci. 2013. The most basal beaked whale *Ninoziphius platyrostris* Muizon, 1983: clues on the evolutionary history of the family Ziphiidae (Cetacea: Odontoceti). Zoological Journal of the Linnean Society 167:569–598.
Lambert, O., C. de Muizon, and G. Bianucci. 2015. A new archaic homodont toothed whale (Mammalia, Cetacea, Odontoceti) from the early Miocene of Peru. Geodiversitas 37:79–108.
Lambert, O., G. Bianucci, M. Urbina, and J. H. Geisler, 2017. A new inioid (Cetacea, Odontoceti, Delphinida) from the Miocene of Peru and the origin of modern dolphin and porpoise families. Zoological Journal of the Linnean Society 179:919–946.
Lambert, O., C. de Muizon, E. Malinverno, C. D. Celma, M. Urbina, and G. Bianucci. 2018. A new odontocete (toothed cetacean) from the Early Miocene of Peru expands the morphological disparity of extinct heterodont dolphins. Journal of Systematic Palaeontology 16:981–1016.
Luo, Z.-X., and K. Marsh. 1996. The petrosal and inner ear structure of a fossil kogiine whale (Odontoceti, Mammalia). Journal of Vertebrate Paleontology 16:328–348.
Mayr, G., J. L. Goedert, and S. A. McLeod. 2013. Partial skeleton of a bony-toothed bird from the late Oligocene/early Miocene of Oregon (USA) and the systematics of Neogene Pelagornithidae. Journal of Paleontology 87:922–929.
McGowen, M. R., M. Spaulding, and J. Gatesy. 2009. Divergence date estimation and a comprehensive molecular tree of extant cetaceans. Molecular Phylogenetics and Evolution 53:891–906.
McGowen, M. R., S. H. Montgomery, C. Clark, and J. Gatesy. 2011. Phylogeny and adaptive evolution of the brain-development gene microcephalin (MCPH1) in cetaceans. BMC Evolutionary Biology 11:98.
Mead, J. G., and R. E. Fordyce. 2009. The therian skull: a lexicon with emphasis on the odontocetes. Smithsonian Contributions to Zoology 627:1–248.
Muizon, C. de. 1984. Les vertébrés de la Formation Pisco (Pérou). Deuxième partie: les Odontocètes (Cetacea, Mammalia) du Pliocène inférieur du Sud-Sacaco. Travaux de l'Institut Français d'Etudes Andines 27:1–188.
Muizon, C. de. 1985. Nouvelles données sur le diphylétisme des Dauphins de rivière (Odontoceti, Cetacea, Mammalia). Comptes rendus de l'Académie des Sciences, Paris 301:359–361.
Muizon, C. de. 1991. A new Ziphiidae (Cetacea) from the Early Miocene of Washington State USA) and phylogenetic analysis of the major groups of odontocetes. Bulletin du Muséum national d'Histoire naturelle, Paris 12:279–326.
Murakami, M., C. Shimada, Y. Hikida, and H. Hirano. 2012. A new basal porpoise, *Pterophocaena nishinoi* (Cetacea, Odontoceti, Delphinoidea), from the upper Miocene of Japan and its phylogenetic relationships. Journal of Vertebrate Paleontology 32:1157–1171.
Nesbitt, E. A. 2018. Cenozoic marine formations of Washington and Oregon: an annotated catalogue. PaleoBios 35:1–20.
Peredo, C. M., M. D. Uhen, and M. D. Nelson. 2018. A new kentriodontid (Cetacea: Odontoceti) from the early Miocene Astoria Formation and a revision of the stem delphinidan family Kentriodontidae. Journal of Vertebrate Paleontology. doi: 10.1080/02724634.2017.1411357.
Prothero, D. R., C. Z. Bitboul, G. W. Moore, and A. R. Niem. 2001a. Magnetic stratigraphy and tectonic rotation of the Oligocene Alsea, Yaquina, and Nye formations, Lincoln County, Oregon; pp. 184–194 in D. R. Prothero (ed.), Magnetic Stratigraphy of the Pacific Coast Cenozoic. Society for Sedimentary Geology Pacific Section, Los Angeles, California.
Prothero, D. R., C. Z. Bitboul, G. W. Moore, and E. J. Moore. 2001b. Magnetic stratigraphy of the lower and middle Miocene Astoria Formation, Lincoln County, Oregon; pp. 272–283 in D. R. Prothero (ed.), Magnetic Stratigraphy of the Pacific Coast Cenozoic. Society for Sedimentary Geology Pacific Section, Los Angeles, California.
Snavely, P. D., Jr., N. S. MacLeod, W. W. Rau, W. O. Addicott, and J. Pearl. 1975. Alsea Formation; an Oligocene marine sedimentary sequence in the Oregon Coast Range. U.S. Geological Survey Bulletin 1395:1–21.
Swofford, D. L. 2001. PAUP*. Phylogenetic Analysis Using Parsimony (*And Other Methods). Version 4b10. Sinauer Associates, Sunderland, Massachusetts.
Tanaka, Y., and R. E. Fordyce. 2014. Fossil dolphin *Otekaikea marplesi* (latest Oligocene, New Zealand) expands the morphological and taxonomic diversity of Oligocene cetaceans. PLoS ONE 9: e107972.
Tanaka, Y., and R. E. Fordyce. 2016. *Papahu*-like fossil dolphin from Kaikoura, New Zealand, helps to fill the Early Miocene gap in the history of Odontoceti. New Zealand Journal of Geology and Geophysics 59:1–17.
Tanaka, Y., and R. E. Fordyce. 2017. *Awamokoa tokarahi*, a new basal dolphin in the Platanistoidea (late Oligocene, New Zealand). Journal of Systematic Palaeontology 15:365–386. doi: 10.1080/14772019.2016.1202339.
Tedford, R. H., L. G. Barnes, and C. E. Ray. 1994. The early Miocene littoral ursoid carnivoran *Kolponomos*: systematics and mode of life. Proceedings of the San Diego Society of Natural History 29:11–32.
Uhen, M. D. 2004. Form, function, and anatomy of *Dorudon atrox* (Mammalia, Cetacea): an archaeocete from the middle to late Eocene of Egypt. University of Michigan Papers on Paleontology 34:1–222.
Uhen, M.D. 2008. New protocetid whales from Alabama and Mississippi, and a new cetacean clade, Pelagiceti. Journal of Vertebrate Paleontology 28:589–593.
Vélez-Juarbe, J. 2017. A new stem odontocete from the late Oligocene Pysht Formation in Washington State, U.S.A. Journal of Vertebrate Paleontology. doi: 10.1080/02724634.2017.1366916.
Wilson, L. E. 1935. Miocene marine mammals from the Bakersfield region, California. Bulletin of the Peabody Museum of Natural History 4:1–143.

Submitted July 11, 2018; revisions received September 13, 2018;
accepted September 15, 2018.
Handling editor: Matthew Borths.